

Study of $\eta - \eta'$ mixing from radiative decay processes

Yun-Hua Chen[†], Zhi-Hui Guo^{‡,§,*}, Han-Qing Zheng[†]

[†] Department of Physics and State Key Laboratory of Nuclear Physics and Technology,
Peking University, Beijing 100871, P. R. China.

[‡] Department of Physics, Hebei Normal University, 050016 Shijiazhuang, P. R. China.

[§] Departamento de Física, Universidad de Murcia, E-30071 Murcia, Spain.

Abstract

We perform a thorough analysis of the $VP\gamma(\gamma^*)$ and $P\gamma\gamma(\gamma^*)$ decays in the resonance chiral theory, where V stand for the vector resonances ρ, K^*, ω, ϕ , P stand for π, K, η, η' and γ^* subsequently decays into lepton pairs. Upon imposing QCD short-distance constraints on resonance couplings, the $\omega \rightarrow \pi\gamma(\gamma^*)$, $\rho \rightarrow \pi\gamma(\gamma^*)$, $K^{*0} \rightarrow K^0\gamma$ processes only depend on one free parameter and $\pi \rightarrow \gamma\gamma(\gamma^*)$ can be completely predicted. The four mixing parameters of the $\eta - \eta'$ system, i.e. two mixing angles θ_8, θ_0 and two decay constants F_8, F_0 , are determined from radiative decays involving η or η' . The higher order low energy constants of the pseudo-Goldstone Lagrangian in the chiral anomaly sector are predicted by integrating out heavy resonances. We also predict the decay widths of $\rho \rightarrow \pi e^+e^-$, $\eta' \rightarrow \gamma e^+e^-$ and $\phi \rightarrow \eta\mu^+\mu^-$, which can be compared with the future measurement in these channels.

PACS: 12.39.Fe, 13.20.Jf, 11.15.Pg

Keywords: $\eta - \eta'$ mixing, chiral Lagrangian, radiative decay of mesons, $1/N_C$ expansion

1 Introduction

To study the properties of η and η' mesons is a very interesting subject in hadron physics. The reasons behind are twofold. First, several experimental collaborations have started or planned programs to launch the measurements of the processes involving the η and η' mesons with high statistics and high precision, such as KLOE [1], Jefferson Lab [2] and BES-III [3]. The huge data sample, for example 63 million events for η decays and 61 million events for η' decays expected at BES-III [3], apparently needs more and finer theoretical work for the analysis. Second, on the theoretical side, η and η' mesons present important information of low energy dynamics of QCD: the mechanism of spontaneously chiral symmetry breaking and the $U_A(1)$ anomaly.

The responsible theory in the low energy region of QCD is Chiral Perturbation Theory (χ PT) [4], whose degrees of freedom are the pseudo-Goldstone mesons, i.e. π, K, η , resulted from the spontaneously chiral symmetry breaking from $SU(3)_L \otimes SU(3)_R$ to $SU(3)_{V=L+R}$. χ PT has been proved to be a very successful effective field theory to describe the low energy physics of QCD [5], that is constructed with respect to chiral symmetry and arranges its effective action in the expansion of momenta and the mass of pseudo-Goldstone bosons. Due to $U_A(1)$ anomaly, η' is prevented to be the ninth pseudo-Goldstone boson. Nevertheless, when the number of the colors in QCD, N_C , becomes large, the effect of $U_A(1)$ anomaly is suppressed. Thus the η' meson becomes the ninth pseudo-Goldstone boson in the large N_C

*guo@um.es

limit [6] and can be incorporated into a chiral Lagrangian. Such an effective theory explicitly including the η' meson extends the standard $SU(3)_L \otimes SU(3)_R$ χ PT to the $U(3)_L \otimes U(3)_R$ version, whose Lagrangian up to $O(p^4)$ has been thoroughly investigated in [7, 8] for the even intrinsic parity sector.

The application of the $U(3)_L \otimes U(3)_R$ χ PT to $\eta - \eta'$ mixing has been performed in the literature [9, 10, 11], where the mixing parameters of η and η' are determined by including higher order corrections, such as the low energy constants (LECs) and the loops. A novel finding after including the higher order contributions in χ PT is that the conventional one-mixing-angle description for $\eta - \eta'$ mixing is not valid any more and two-mixing-angle scheme is then proposed in [10]. In our current discussion, instead of working in more detail in the top-down method to address the $\eta - \eta'$ mixing problem, we are going to determine the mixing couplings in a bottom-up way, i.e., we assume the validity of the two-mixing-angle description and then directly fit them using experimental data from the relevant physical processes that involve η or η' . We will focus on the radiative decay processes in the present work, since they can provide a large sample of data [12] that allows us to better extract the $\eta - \eta'$ mixing information and they are less contaminated by the strong final state interaction comparing with the hadronic decay modes, such as $\eta' \rightarrow \eta\pi\pi$ [13].

Among the radiative decay processes with η or η' meson in the low energy sector, many of them consist of one vector resonance, such as $\phi \rightarrow \eta\gamma$, $\eta' \rightarrow \omega\gamma$, and so on [12]. Apparently, these processes are already beyond the validity region of χ PT due to the appearance of the heavy vector resonances. It is by no means trivial to systematically include the heavy vector resonances in χ PT, since the expansion parameters of χ PT are no longer valid after the inclusion of the heavy multiplet of resonances. Nevertheless, the framework developed in Ref. [14], named Resonance Chiral Theory (R χ T), has been proven to be useful and may shed light on the proper construction of the Lagrangian theory that one could use to describe the dynamics with both pseudo-Goldstone mesons and resonances. It can be better understood within the framework of the large N_C QCD as theory of hadrons [15]. While in the strict large N_C QCD there is an infinite number of zero-width hadrons in the spectrum, in practical realization one usually needs to truncate the infinite tower of resonances to the lowest multiplet for each quantum number. There has been a large amount of research works based on this approximation, varying from determination of the χ PT LECs [16, 17] to the study of tau decays [18, 19, 20] and Green functions of QCD currents [21, 22, 23, 24, 25].

R χ T, although well respecting chiral symmetry and constructed in the guide of $1/N_C$ expansion, is still lacking of QCD dynamics at the high energy scale where the continuum is reached and perturbative QCD is the responsible theory. Thus it is crucial to match the behaviors of the effective field theory and QCD at high momentum transfer to implement as many QCD features as possible. Research along this line indeed has been intensively performed in many works [21, 22, 23, 24, 25]. This procedure directly results in the constraints on the resonance couplings and hence makes the theory more predictable.

In the present work, we utilize R χ T to analyze the $VP\gamma(\gamma^*)$ and $P\gamma\gamma(\gamma^*)$ processes. Comparing with the work in Ref. [25], we generalize the R χ T Lagrangian with the octet of pseudo-Goldstone mesons to the version with nonet, thus allowing us to study the processes with η' meson. Our work is also especially devoted to the determination of the $\eta - \eta'$ mixing parameters by fitting data, which we will explain in detail later in the text.

We organize the article as follow. A mini-review on $\eta - \eta'$ mixing is given in Section 2. The structure of the relevant R χ T Lagrangian is elaborated in Section 3. The computation of the decay amplitudes of $VP\gamma(\gamma^*)$ and $P\gamma\gamma(\gamma^*)$ is noted in Section 4. The QCD short distance constraints are discussed in Section 5. Phenomenology discussion is given in Section 6 and we conclude in Section 7.

2 Mini-review on $\eta - \eta'$ mixing

$\eta - \eta'$ mixing is an interesting subject in hadron physics. In the literature, the mixing angles have been defined with respect to different bases: the octet-singlet flavour basis and the quark flavour basis. For our purpose, we will always adopt the octet-singlet flavour basis to define the mixing angles throughout this article. The two-mixing-angle description has been proposed to settle the $\eta - \eta'$ mixing [10], going beyond the old one-mixing-angle description [26]. The requirement of the two mixing angles can be better understood in the χ PT frame. The leading order Lagrangian of $U(3)_L \otimes U(3)_R$ χ PT is

$$\mathcal{L}^{(0)} = \frac{F^2}{4} \langle u_\mu u^\mu \rangle + \frac{F^2}{4} \langle \chi_+ \rangle + \frac{F^2}{3} M_0^2 \ln^2 \det u, \quad (1)$$

where

$$u(x) = \exp(i \frac{\Phi(x)}{\sqrt{2}F}), \quad (2)$$

$$\Phi(x) = \begin{pmatrix} \frac{\sqrt{3}\pi^0 + \eta_8 + \sqrt{2}\eta_1}{\sqrt{6}} & \pi^+ & K^+ \\ \pi^- & \frac{-\sqrt{3}\pi^0 + \eta_8 + \sqrt{2}\eta_1}{\sqrt{6}} & K^0 \\ K^- & \bar{K}^0 & \frac{-2\eta_8 + \sqrt{2}\eta_1}{\sqrt{6}} \end{pmatrix}. \quad (3)$$

The last term in Eq.(1) represents the $U_A(1)$ anomaly of QCD, which gives rise to the singlet η_1 mass, M_0 . F is the value of the pseudo-Goldstone decay constant in the chiral limit, with the normalization of $F_\pi = 92.4$ MeV. For other chiral building blocks, see Ref. [14] and references therein.

At leading order, only one mixing angle is needed to diagonalize the octet η_8 and the singlet η_1 to get the mass eigenstates η and η' , since there is only one mixing term in the mass sector. However, the higher order corrections, including the loop contributions and the LECs from the higher order Lagrangian, contribute not only to the mixing of mass but also to the mixing of kinetic term. In order to get the physical eigenstates of η and η' , one needs three steps: first to diagonalize the kinetic term, then to perform the normalization of each field and to diagonalize the mass term in the end, which indicates four parameters, i.e. two angles and two normalization constants, are needed in this procedure. It has been shown in Ref. [10, 11] the mixing can be parameterized as,

$$\begin{pmatrix} \eta \\ \eta' \end{pmatrix} = \frac{1}{F} \begin{pmatrix} F_8 \cos \theta_8 & -F_0 \sin \theta_0 \\ F_8 \sin \theta_8 & F_0 \cos \theta_0 \end{pmatrix} \begin{pmatrix} \eta_8 \\ \eta_1 \end{pmatrix}, \quad (4)$$

where F_8 and F_0 correspond to the weak decay constants of the axial octet and singlet currents, respectively. By setting $F_8 = F_0 = F$ and $\theta_0 = \theta_8$ in Eq.(4), the conventional one-mixing-angle scheme can be recovered.

The works presented in Refs. [10, 11, 9] are devoted to the determination of the mixing parameters $F_8, F_0, \theta_8, \theta_0$ by including the higher order corrections in $U(3)$ χ PT. Recently assorted methods along this line have been done to settle the $\eta - \eta'$ mixing in [27, 28]. As already advertised in the Introduction, instead of considering more of higher order corrections to calculate the mixing parameters, we will first adopt the two-mixing-angle scheme described in Eq.(4) for the $\eta - \eta'$ system and then determine the unknown mixing parameters phenomenologically. Similar works within this context have been carried out in Refs. [29, 30, 31, 32, 33, 34, 35, 36, 37, 38, 39], which confirm the robustness of the two-mixing-angle description scheme. In the present work we would like to readdress the similar processes, such as the $VP\gamma$ and $P\gamma\gamma$, in the framework of $R\chi$ T. The advantage of $R\chi$ T is that it preserves the chiral symmetry

in the low energy sector, respects the high energy behavior of QCD and incorporates all of the symmetry allowed operators in the construction, in contrast to the previous works where only a single constant term is introduced to describe the interaction vertex for $VP\gamma$. In addition, we perform a global fit by including all of the experimental available processes with the types of $V \rightarrow P\gamma$, $P \rightarrow V\gamma$ and $P \rightarrow \gamma\gamma$ and also discuss the processes with an off-shell photon decaying into lepton pairs: $V \rightarrow Pl^+l^-$, $P \rightarrow Vl^+l^-$ and $P \rightarrow \gamma l^+l^-$, where V stand for ρ, ω, ϕ, K^* and P stand for π, K, η, η' .

3 The relevant Lagrangian of $R\chi T$

The resonance chiral effective Lagrangian describing vector-photon-pseudoscalar and vector-vector-pseudoscalar vertexes with the vector resonance in the antisymmetric tensor field formulation has been given in Ref. [25], in which only the octet of the pseudo-Goldstone mesons is included. Using the constraints derived from the short distance behavior of QCD, the Lagrangian has been used to predict the decay widths of $\omega \rightarrow \pi\gamma$ and $\pi \rightarrow \gamma\gamma$, which are in good agreement with the experimental data [12]. In order to study the similar processes with η' , we need to generalize the existing resonance Lagrangian with the pseudo-Goldstone octet to the one involving the singlet state in addition to the octet. Thanks to large N_C QCD, this can be simply accomplished by extending the content of the unitary matrix $u(x)$, defined in Eq.(2), from the octet to nonet. In addition, new operators may appear too, as the unitary matrix $u(x)$ is no longer traceless after the inclusion of the singlet.

We recall the procedure to construct the $U(3)$ χ PT Lagrangian [7, 8] before illustrating how to build the new operators in the resonance chiral Lagrangian. The key ingredient introduced to construct the $U(3)$ χ PT operators is the $1/N_C$ expansion, in addition to the conventional expansion of momentum and the quark mass, which is usually named as the triple expansion scheme, i.e. $\delta \sim p^2 \sim m_q \sim 1/N_C$. It also turns out to be useful when building resonance Lagrangian with the singlet η_1 as an explicit degree of freedom [40, 41].

As already mentioned previously, in this article we focus on the radiative decay processes with the types of $VP\gamma$ and $P\gamma\gamma$, belonging to the odd intrinsic parity process describing two vector subjects (photon or vector resonance) and one pseudoscalar. Guided by the triple expansion scheme, the lowest order Lagrangian in the odd intrinsic parity sector is in fact the chiral anomaly formulated in the Wess-Zumino-Witten (WZW) action [42, 43], with the order of $\mathcal{O}(p^4, N_C)$. The relevant piece in our discussion can be written in the following way

$$\mathcal{L}_{WZW} = -\frac{\sqrt{2}N_C}{8\pi^2 F} \varepsilon_{\mu\nu\rho\sigma} \langle \Phi \partial^\mu v^\nu \partial^\rho v^\sigma \rangle, \quad (5)$$

where to get the photon field one needs to take $v_\mu = -eQ A_\mu$ and the electric charge matrix of the light quarks with three flavours is $Q = \text{Diag}\{\frac{2}{3}, -\frac{1}{3}, -\frac{1}{3}\}$.

The higher order Lagrangians can be categorized into two types: the higher order chiral anomaly pseudo-Goldstone Lagrangian and the Lagrangian with vector resonances. It is known that the higher order operators in the pure Goldstone Lagrangian encode the information of heavier degrees of freedom that have been integrated out. To avoid the double counting in $R\chi T$, the LECs of the higher order Lagrangian in the pseudo-Goldstone sector is usually assumed to be completely saturated by the heavy resonance states and thus the higher order operators in the pure pseudo-Goldstone sector can be dismissed, which works at least pretty well up to the $\mathcal{O}(p^4)$ level in the even intrinsic sector [14]. It is pointed out in Ref. [44] to fulfil this procedure it is necessary to use the antisymmetric formalism to describe the vector resonances. Though analogous analysis has not been carried out in the odd intrinsic parity sector, the resonance saturation assumption is utilized to construct the resonance Lagrangian in Ref. [25] and we generalize the discussion by including the singlet pseudo-Goldstone within the triple expansion scheme.

If the operator is written in terms of $\tilde{u}(x)$, $\tilde{u}(x) \in U(3)$, it obeys the canonical large N_C counting rules: terms with a single trace are of order N_C while one additional trace reduces its order by unity of $1/N_C$. The factor of $\ln(\det \tilde{u})$ also leads to a suppression of $1/N_C$ [7, 8, 40]. The interacting vertex involving resonances and pseudo-Goldstones has the general structure at leading order of N_C

$$\mathcal{O}_i \sim \langle R_1 R_2 \dots R_j \chi^{(n)}(\varphi) \rangle, \quad (6)$$

where $\chi^n(\varphi)$ denotes the chiral tensor that only incorporates pseudo-Goldstone bosons and the auxiliary fields with the chiral order $\mathcal{O}(p^n)$. For the odd intrinsic parity sector, it has been shown two types of vector resonance operators are relevant: $\langle V\chi^{(4)}(\varphi) \rangle$ and $\langle VV\chi^{(2)}(\varphi) \rangle$ in the case of $u(x) \in SU(3)$. When the singlet pseudo-Goldstone is taken into account, i.e. $\tilde{u}(x) \in U(3)$, two new operators with the same chiral counting order within the triple expansion scheme show up: $\langle V\chi^{(2)}(\varphi) \rangle \ln(\det \tilde{u})$ and $\langle VV \rangle \ln(\det \tilde{u})$. The complete Lagrangians are found to be

$$\begin{aligned} \tilde{\mathcal{L}}_{VJP} = & \frac{\tilde{c}_1}{M_V} \varepsilon_{\mu\nu\rho\sigma} \langle \{V^{\mu\nu}, \tilde{f}_+^{\rho\alpha}\} \nabla_\alpha \tilde{u}^\sigma \rangle \\ & + \frac{\tilde{c}_2}{M_V} \varepsilon_{\mu\nu\rho\sigma} \langle \{V^{\mu\alpha}, \tilde{f}_+^{\rho\sigma}\} \nabla_\alpha \tilde{u}^\nu \rangle \\ & + \frac{i\tilde{c}_3}{M_V} \varepsilon_{\mu\nu\rho\sigma} \langle \{V^{\mu\nu}, \tilde{f}_+^{\rho\sigma}\} \tilde{\chi}_- \rangle \\ & + \frac{i\tilde{c}_4}{M_V} \varepsilon_{\mu\nu\rho\sigma} \langle V^{\mu\nu} [\tilde{f}_-^{\rho\sigma}, \tilde{\chi}_+] \rangle \\ & + \frac{\tilde{c}_5}{M_V} \varepsilon_{\mu\nu\rho\sigma} \langle \{ \nabla_\alpha V^{\mu\nu}, \tilde{f}_+^{\rho\alpha} \} \tilde{u}^\sigma \rangle \\ & + \frac{\tilde{c}_6}{M_V} \varepsilon_{\mu\nu\rho\sigma} \langle \{ \nabla_\alpha V^{\mu\alpha}, \tilde{f}_+^{\rho\sigma} \} \tilde{u}^\nu \rangle \\ & + \frac{\tilde{c}_7}{M_V} \varepsilon_{\mu\nu\rho\sigma} \langle \{ \nabla^\sigma V^{\mu\nu}, \tilde{f}_+^{\rho\alpha} \} \tilde{u}_\alpha \rangle \\ & - i\tilde{c}_8 M_V \sqrt{\frac{2}{3}} \varepsilon_{\mu\nu\rho\sigma} \langle V^{\mu\nu} \tilde{f}_+^{\rho\sigma} \rangle \ln(\det \tilde{u}), \end{aligned} \quad (7)$$

$$\begin{aligned} \tilde{\mathcal{L}}_{VVP} = & \tilde{d}_1 \varepsilon_{\mu\nu\rho\sigma} \langle \{V^{\mu\nu}, V^{\rho\alpha}\} \nabla_\alpha \tilde{u}^\sigma \rangle \\ & + i\tilde{d}_2 \varepsilon_{\mu\nu\rho\sigma} \langle \{V^{\mu\nu}, V^{\rho\sigma}\} \tilde{\chi}_- \rangle \\ & + \tilde{d}_3 \varepsilon_{\mu\nu\rho\sigma} \langle \{ \nabla_\alpha V^{\mu\nu}, V^{\rho\alpha} \} \tilde{u}^\sigma \rangle \\ & + \tilde{d}_4 \varepsilon_{\mu\nu\rho\sigma} \langle \{ \nabla^\sigma V^{\mu\nu}, V^{\rho\alpha} \} \tilde{u}_\alpha \rangle \\ & - i\tilde{d}_5 M_V^2 \sqrt{\frac{2}{3}} \varepsilon_{\mu\nu\rho\sigma} \langle V^{\mu\nu} V^{\rho\sigma} \rangle \ln(\det \tilde{u}), \end{aligned} \quad (8)$$

where we introduce tildes to the objects involving the Goldstone nonet to distinguish the one with octet. Comparing with Ref. [25], the new operators are

$$\begin{aligned} \tilde{O}_{VJP}^8 &= -i\tilde{c}_8 M_V \sqrt{\frac{2}{3}} \varepsilon_{\mu\nu\rho\sigma} \langle V^{\mu\nu} \tilde{f}_+^{\rho\sigma} \rangle \ln(\det \tilde{u}), \\ \tilde{O}_{VVP}^5 &= -i\tilde{d}_5 M_V^2 \sqrt{\frac{2}{3}} \varepsilon_{\mu\nu\rho\sigma} \langle V^{\mu\nu} V^{\rho\sigma} \rangle \ln(\det \tilde{u}). \end{aligned} \quad (9)$$

We point out the above operators are only complete for the case with one pseudoscalar field. In the case with more pseudoscalar states, Ref. [25] has been generalized in Ref. [45] to include all of the relevant resonance operators that can contribute to the $\mathcal{O}(p^6)$ χ PT LECs in the odd intrinsic parity Lagrangian.

The relevant Lagrangian in the even intrinsic parity sector, describing the vector resonance and photon transition vertex, is [14]

$$\mathcal{L}_2^V = \frac{F_V}{2\sqrt{2}} \langle V_{\mu\nu} \tilde{f}_+^{\mu\nu} \rangle, \quad (10)$$

and the kinetic term for the vector resonance in the antisymmetric formulation reads [14]

$$\mathcal{L}_{kin}(V) = -\frac{1}{2} \langle \nabla^\lambda V_{\lambda\mu} \nabla_\nu V^{\nu\mu} - \frac{M_V^2}{2} V_{\mu\nu} V^{\mu\nu} \rangle, \quad (11)$$

where the nonet of the vector resonances resemble the flavor structure of the pseudo-Goldstone mesons

$$V_{\mu\nu} = \begin{pmatrix} \frac{1}{\sqrt{2}}\rho^0 + \frac{1}{\sqrt{6}}\omega_8 + \frac{1}{\sqrt{3}}\omega_1 & \rho^+ & K^{*+} \\ \rho^- & -\frac{1}{\sqrt{2}}\rho^0 + \frac{1}{\sqrt{6}}\omega_8 + \frac{1}{\sqrt{3}}\omega_1 & K^{*0} \\ K^{*-} & \bar{K}^{*0} & -\frac{2}{\sqrt{6}}\omega_8 + \frac{1}{\sqrt{3}}\omega_1 \end{pmatrix}_{\mu\nu}. \quad (12)$$

For the vector resonances ω and ϕ , we assume the ideal mixing throughout this paper:

$$\begin{aligned} \omega_1 &= \sqrt{\frac{2}{3}}\omega - \sqrt{\frac{1}{3}}\phi, \\ \omega_8 &= \sqrt{\frac{2}{3}}\phi + \sqrt{\frac{1}{3}}\omega. \end{aligned} \quad (13)$$

The relevant R χ T Lagrangian to our discussion can be summarized as follow

$$\mathcal{L} = \mathcal{L}_{WZW} + \mathcal{L}_{kin}^V + \mathcal{L}_2^V + \tilde{\mathcal{L}}_{VJP} + \tilde{\mathcal{L}}_{VVP}. \quad (14)$$

4 Theoretical calculation of the radiative decay amplitudes

In accord with the Lorentz symmetry, the general amplitude for the radiative decay $V(q) \rightarrow P(p)\gamma^*(k)$ can be written as:

$$i\mathcal{M}_{V \rightarrow P\gamma^*} = i e \varepsilon_{\mu\nu\rho\sigma} \epsilon_V^\mu \epsilon_{\gamma^*}^\nu q^\rho k^\sigma F_{V \rightarrow P\gamma^*}(Q^2), \quad (15)$$

where ϵ_V and ϵ_{γ^*} denote the polarization vectors of the vector resonance and the off-shell photon respectively; the transferred momentum square is defined as $Q^2 = -k^2$. In the case of the on-shell photon, one only needs to replace ϵ_{γ^*} with the on shell polarization vector ϵ_γ and impose the real photon condition $Q^2 = -k^2 = 0$. Thus the decay widths of $V \rightarrow P\gamma$ and $P \rightarrow V\gamma$ are found to be:

$$\Gamma(V \rightarrow P\gamma) = \frac{1}{3} \alpha \left(\frac{M_V^2 - M_P^2}{2M_V} \right)^3 |F_{V \rightarrow P\gamma^*}(0)|^2, \quad (16)$$

$$\Gamma(P \rightarrow V\gamma) = \alpha \left(\frac{M_P^2 - M_V^2}{2M_V} \right)^3 |F_{P \rightarrow V\gamma^*}(0)|^2, \quad (17)$$

where $\alpha = e^2/4\pi$ stands for the fine structure constant and the form factor $F_{P \rightarrow V\gamma^*}(Q^2)$ can be defined in the same way as Eq.(15)

$$i\mathcal{M}_{P(p) \rightarrow V(q)\gamma^*(k)} = i e \varepsilon_{\mu\nu\rho\sigma} \epsilon_V^\mu \epsilon_{\gamma^*}^\nu q^\rho k^\sigma F_{P \rightarrow V\gamma^*}(Q^2 = -k^2). \quad (18)$$

The decay width of $P \rightarrow \gamma\gamma$ can be calculated

$$\Gamma(P \rightarrow \gamma\gamma) = \frac{1}{4}\pi\alpha^2 M_P^3 |F_{P \rightarrow \gamma\gamma^*}(0)|^2, \quad (19)$$

where the form factor $F_{P \rightarrow \gamma\gamma^*}(Q^2)$ is defined in an analogous way as Eq.(18) by replacing the vector resonance V with an on-shell photon.

Next we use the resonance chiral Lagrangian described previously to calculate the decay widths and transition form factors defined above, which represent one of our main results in this work. We only consider the tree-level amplitudes here. The relevant Feynman diagrams to the radiative $VP\gamma^*$ transitions are displayed in Fig. 1. It is worth pointing out in the celebrated vector meson dominant(VMD) model only the type (b) diagram in Fig. 1 shows up. For the radiative transition $P \rightarrow \gamma\gamma^*$, the Feynman diagrams are displayed in Fig. 2.

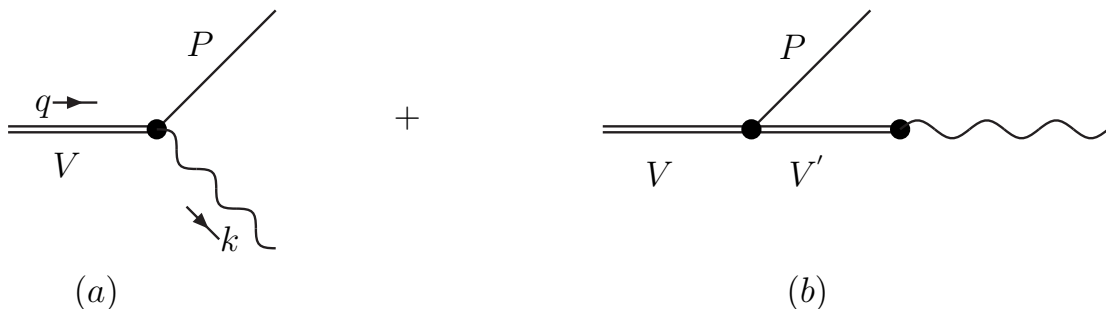


Figure 1: Two types of Feynman diagrams for the processes $VP\gamma^*$.

Since the expressions for the various decay widths, such as $V \rightarrow P\gamma$, $P \rightarrow V\gamma$ and $P \rightarrow \gamma\gamma$, are rather lengthy, we relegate them in Appendix A. The form factors of $F_{P \rightarrow \gamma\gamma^*}(s)$ and $F_{V \rightarrow P\gamma^*}(s)$ can be found in Appendix B. The kinematics and amplitudes of $V \rightarrow P\gamma^* \rightarrow Pl^-l^+$, $P \rightarrow V\gamma^* \rightarrow Vl^-l^+$ and $P \rightarrow \gamma\gamma^* \rightarrow \gamma l^-l^+$, with the lepton $l = e, \mu$ are given in Appendix C.

5 Short distance constraints from QCD

Given R χ T being the dual theory of QCD in the resonance region, the couplings appearing in the resonance chiral Lagrangian can not be completely free, since there is only one parameter in QCD: Λ_{QCD} and the heavy quark masses. To fix the resonance couplings in terms of them requires solving the nonperturbative dynamics of QCD from the first principle, which is exactly the reason that the chiral effective field theory arises. Nevertheless, in the last decades, a sufficient way to implement the short distance feature of QCD has been developed, that is to match the operator product expansion(OPE) of Green functions of QCD currents which are of order parameter of the chiral symmetry breaking to the same quantity calculated within the resonance chiral Lagrangian [21, 22, 23, 24, 25]. Through this procedure, one could constrain sufficiently the resonance couplings in certain cases.

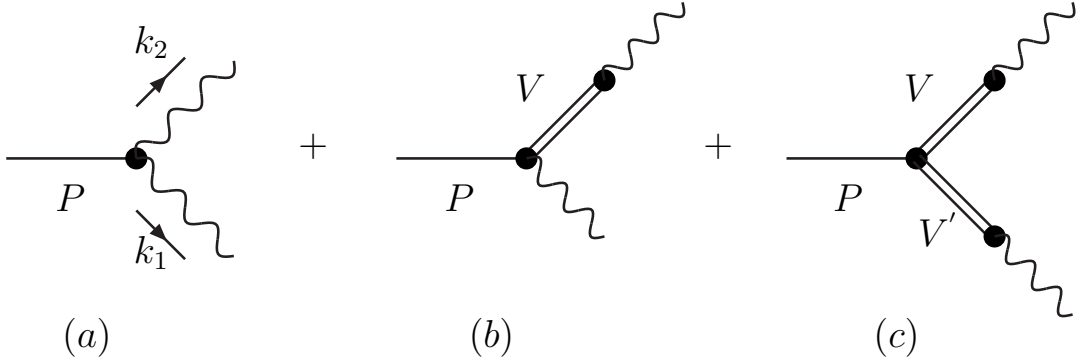


Figure 2: Feynman diagrams for $P\gamma\gamma^*$

The three-point Green function with vector-vector-pseudoscalar QCD currents has been studied in different works. Ref. [21] is devoted to the analysis of $P \rightarrow \gamma\gamma$ by taking into the higher order Goldstone chiral Lagrangian. The focus of Ref. [24] is to estimate the resonance contributions to the $\mathcal{O}(p^6)$ LECs of χ PT by using the vector formalism to describe the vector resonances, while Ref. [45] exploits the antisymmetric tensor formalism to incorporate the vector resonances. In Ref. [25], the VVP Green function has been analyzed by using the antisymmetric tensor representation for the vector resonances and the phenomenology study focused on the radiative processes of $\omega \rightarrow \pi\gamma$ and $\pi \rightarrow \gamma\gamma$. Our discussion in this section is devoted to the generalized study of VVP Green function given in [25] by extending the content of pseudo-Goldstone bosons from the octet case to the nonet one, i.e. $u(x) \in SU(3) \rightarrow \tilde{u}(x) \in U(3)$.

The VVP Green function is defined as

$$\int d^4x \int d^4y e^{i(p \cdot x + q \cdot y)} \langle 0 | T [V_\mu^a(x) V_\nu^b(y) P^c(0)] | 0 \rangle = d^{abc} \epsilon_{\mu\nu\alpha\beta} p^\alpha q^\beta \Pi_{VVP}(p^2, q^2, r^2), \quad (20)$$

where the flavor indices are $a, b, c = 0, \dots, 8$; r_μ is defined as $r_\mu = -(p + q)_\mu$; the vector and pseudoscalar currents are given by

$$V_\mu^a(x) = (\bar{\psi} \gamma_\mu \frac{\lambda^a}{2} \psi)(x), \quad P^a(x) = (\bar{\psi} i \gamma_5 \frac{\lambda^a}{2} \psi)(x). \quad (21)$$

Taking $c = 0$, one can get the singlet pseudoscalar current and $\Pi_{VVP}^{(0)}$ can be defined correspondingly. Although the evaluation of the singlet $\Pi_{VVP}^{(0)}$ and the octet $\Pi_{VVP}^{(8)}$ in the intermediate energy region could lead to different results due to the $U_A(1)$ anomaly, their asymptotic behaviors coincide in the chiral limit and at leading order of $1/N_C$ [21]

$$\begin{aligned} \lim_{\lambda \rightarrow \infty} \Pi_{VVP}^{(8)}[(\lambda p)^2, (\lambda q)^2, (\lambda p + \lambda q)^2] &= \lim_{\lambda \rightarrow \infty} \Pi_{VVP}^{(0)}[(\lambda p)^2, (\lambda q)^2, (\lambda p + \lambda q)^2] = \\ &= \frac{\langle \bar{\psi} \psi \rangle_0}{2\lambda^4} \frac{p^2 + q^2 + r^2}{p^2 q^2 r^2} [1 + \mathcal{O}(\alpha_S)] + \mathcal{O}\left(\frac{1}{\lambda^6}\right). \end{aligned} \quad (22)$$

Next let us focus on the calculation of the VVP Green function within $R\chi T$. Since the new operators given in Eq.(9) only contribute to the singlet $\Pi_{VVP}^{(0)}$, the matching of the octet Green function $\Pi_{VVP}^{(8)}$ does not lead to any new constraints on the resonance couplings, comparing with the results in [25]. So we concentrate on the evaluation of the singlet VVP Green function $\Pi_{VVP}^{(0)}$ in $R\chi T$ and the result is found to be

$$\begin{aligned}
\Pi_{VVP}^{(0)}(p^2, q^2, r^2) = & -\frac{\langle\bar{\psi}\psi\rangle_0}{F^2} \left\{ -4F_V^2 \frac{(\tilde{d}_1 - \tilde{d}_3)r^2 + \tilde{d}_3(p^2 + q^2)}{(M_V^2 - p^2)(M_V^2 - q^2)(M_0^2 - r^2)} \right. \\
& + 2\sqrt{2} \frac{F_V}{M_V} \frac{(\tilde{c}_1 + \tilde{c}_2 - \tilde{c}_5)r^2 + (\tilde{c}_2 + \tilde{c}_5 - \tilde{c}_1 - 2\tilde{c}_6)p^2 + (\tilde{c}_1 - \tilde{c}_2 + \tilde{c}_5)q^2}{(M_0^2 - r^2)(M_V^2 - p^2)} \\
& + 2\sqrt{2} \frac{F_V}{M_V} \frac{(\tilde{c}_1 + \tilde{c}_2 - \tilde{c}_5)r^2 + (\tilde{c}_2 + \tilde{c}_5 - \tilde{c}_1 - 2\tilde{c}_6)q^2 + (\tilde{c}_1 - \tilde{c}_2 + \tilde{c}_5)p^2}{(M_0^2 - r^2)(M_V^2 - q^2)} \\
& + \frac{32F_V^2 \tilde{d}_2}{(M_V^2 - p^2)(M_V^2 - q^2)} - \frac{16\sqrt{2}F_V \tilde{c}_3}{M_V} \left(\frac{1}{M_V^2 - p^2} + \frac{1}{M_V^2 - q^2} \right) + \frac{N_C}{8\pi^2(M_0^2 - r^2)} \\
& + 4\sqrt{3} \tilde{c}_8 M_V F_V \left[\frac{1}{(M_V^2 - q^2)(M_0^2 - r^2)} + \frac{1}{(M_V^2 - p^2)(M_0^2 - r^2)} \right] \\
& \left. - 2\sqrt{6} \frac{\tilde{d}_5 F_V^2 M_V^2}{(M_V^2 - p^2)(M_V^2 - q^2)(M_0^2 - r^2)} \right\}. \tag{23}
\end{aligned}$$

We stress that the above expression for $\Pi_{VVP}^{(0)}$ is worked out in the chiral limit. Due to the $U_A(1)$ anomaly, the singlet pseudoscalar η_1 gains the non-vanishing mass M_0 even at the chiral limit. Although the η_1 mass M_0 is suppressed by $1/N_C$, its value is not a small quantity, which is even higher than the lowest vector resonance mass M_V [26]. Hence to take this effect into account we have introduced the non-vanishing mass for η_1 in the calculation of the $\Pi_{VVP}^{(0)}$ function within $R\chi T$.

Matching the result evaluated from OPE of the singlet VVP Green function displayed in Eq.(22) to the same quantity evaluated within $R\chi T$, which is given in Eq.(23), leads to the following constraints

$$4\tilde{c}_3 + \tilde{c}_1 = 0, \tag{24}$$

$$\tilde{c}_1 - \tilde{c}_2 + \tilde{c}_5 = 0, \tag{25}$$

$$\tilde{c}_5 - \tilde{c}_6 = \frac{N_C}{64\pi^2} \frac{M_V}{\sqrt{2}F_V}, \tag{26}$$

$$\tilde{d}_1 + 8\tilde{d}_2 - \tilde{d}_3 = \frac{F^2}{8F_V^2}, \tag{27}$$

$$\tilde{d}_3 = -\frac{N_C}{64\pi^2} \frac{M_V^2}{F_V^2} + \frac{F^2}{8F_V^2} - \frac{\sqrt{3}M_V}{F_V} \tilde{c}_8 - \frac{\sqrt{2}M_0^2}{M_V F_V} \tilde{c}_1. \tag{28}$$

We find the above constraints are all consistent with the ones given in [25], except for the relation of \tilde{d}_3 . The consistent condition for the results of \tilde{d}_3 from the octet and singlet cases requires

$$\tilde{c}_8 = -\frac{\sqrt{2}M_0^2}{\sqrt{3}M_V^2} \tilde{c}_1. \tag{29}$$

So in the numerical discussion, we will take this constraint for \tilde{c}_8 .

There is another well known approach to address the features of form factors corresponding to exclusive processes of QCD with high momenta transfer, which was developed within the parton description scheme

for the hadrons in Ref. [46]. The relevant one to our present discussion is the photon meson transition form factor $F_{\pi\gamma}(Q^2)$, which can match the form factor defined in Eq.(15) by applying the time reversal and replacing the vector resonance with the on-shell photon. Although different approaches have predicted different asymptotic behaviors of $F_{\pi\gamma}(Q^2)$ at the order of Q^{-2} , for example

$$\begin{aligned} F_{\pi\gamma}(Q^2 \rightarrow \infty) &= -\frac{F}{Q^2}, \\ F_{\pi\gamma}(Q^2 \rightarrow \infty) &= -\frac{2F}{3Q^2}, \\ F_{\pi\gamma}(Q^2 \rightarrow \infty) &= -\frac{F}{3Q^2}, \end{aligned} \quad (30)$$

which are noted in Refs [46][47][48] respectively, they agree at the order of Q^0 , indicating the form factor behaving smoothly at the high momentum transfer, i.e. $F_{\pi\gamma}(Q^2 \rightarrow \infty) \rightarrow 0$. So the most conservative constraint would be just to impose the vanishing condition for the constant term in the form factor, i.e. to demand the coefficient of Q^0 being zero. The explicit expression for the form factor of $\pi\gamma\gamma^*$ can be found in Appendix C and the corresponding high energy constraint from the order of Q^0 is

$$\begin{aligned} \tilde{c}_1 - \tilde{c}_2 + \tilde{c}_5 &= 0, \\ \tilde{c}_5 - \tilde{c}_6 &= \frac{F_V}{\sqrt{2}M_V}\tilde{d}_3 + \frac{N_C M_V}{32\sqrt{2}\pi^2 F_V}, \end{aligned} \quad (31)$$

and the corresponding constraint from the form factor of $\omega\pi\gamma^*$, which is also given in Appendix C, leads to

$$\begin{aligned} \tilde{c}_1 - \tilde{c}_2 + \tilde{c}_5 &= 0, \\ \tilde{c}_5 - \tilde{c}_6 &= -\frac{F_V}{\sqrt{2}M_V}\tilde{d}_3. \end{aligned} \quad (32)$$

Combining Eq.(31) and Eq.(32), we have the following relations

$$\begin{aligned} \tilde{c}_1 - \tilde{c}_2 + \tilde{c}_5 &= 0, \\ \tilde{c}_5 - \tilde{c}_6 &= \frac{N_C}{64\pi^2} \frac{M_V}{\sqrt{2}F_V}, \\ \tilde{d}_3 &= -\frac{N_C}{64\pi^2} \frac{M_V^2}{F_V^2}. \end{aligned} \quad (33)$$

When discussing the high energy constraints, we take the chiral limit and $U(3)$ symmetry for the vector resonances. In this case, the physical states η and η' are represented by the flavour eigenstates η_8 and η_1 , respectively. So in the chiral limit, the constraints from the other processes with octet pseudoscalar mesons lead to the same results, while the process involving the singlet pseudoscalar η_1 could lead to different results as we keep the $U_A(1)$ anomaly effect, i.e. the non-vanishing η_1 mass, in the deriving the high energy constraint. The explicit result from the analysis of the $\eta_1\gamma\gamma^*$ form factor is

$$\begin{aligned} \tilde{c}_1 - \tilde{c}_2 + \tilde{c}_5 &= 0, \\ \tilde{c}_5 - \tilde{c}_6 &= \frac{N_C}{64\pi^2} \frac{M_V}{\sqrt{2}F_V}, \\ \tilde{d}_3 &= -\frac{N_C}{64\pi^2} \frac{M_V^2}{F_V^2} - \frac{\sqrt{3}M_V}{F_V}\tilde{c}_8 - \frac{\sqrt{2}M_0^2}{M_V F_V}\tilde{c}_1, \end{aligned} \quad (34)$$

To demand the consistency of the results from $\pi\gamma\gamma^*$ and $\eta_1\gamma\gamma^*$, we arrive at the same constraint in Eq.(29).

Notice that the only inconsistency from the OPE and form factors is the relation of \tilde{d}_3 , although fewer constraints are obtained in the analysis of form factors. This observation has been confirmed in other processes [19, 20]. The fact that only one multiplet of resonances was unable to fulfill all the high energy constraints from OPE and the corresponding form factors was already noticed [24, 23, 49]. In this work, we will take the result for \tilde{d}_3 in Eq.(33) obtained from the high energy constraint of form factor, which is more related to the processes we are discussing. To reduce the free parameters as many as possible in the phenomenology discussion, we also exploit the constraints in Eq.(24) and Eq.(27) obtained from the OPE analysis. In summary, the high energy constraints we are going to use in the following discussion are those in Eq.(24), Eq.(27), Eq.(29) and Eq.(33).

6 Phenomenology discussion

Although we can fix some parameters through the short distance constraints from QCD in the previous section, some of the resonance couplings appearing in the decay widths given in Appendix are still unconstrained. So we need to fit the unknown resonance couplings, such as \tilde{c}_3, \tilde{d}_2 and \tilde{d}_5 , together with the $\eta - \eta'$ mixing parameters θ_0, θ_8, F_0 and F_8 . For the mass of vector resonances in the chiral limit M_V , one can safely estimate its value by M_ρ , the mass of $\rho(770)$ [17]. While for the parameter F_V , describing the transition strength of the neutral vector resonances and photon, its value is still a somewhat controversial subject and several solutions have been proposed in different works. In the pioneer work to discuss the high energy constraints in R χ T [44], $F_V = \sqrt{2}F$ was predicted by combining the high energy constraints from the pion vector and axial-vector form factors within the minimal R χ T Lagrangian at leading order of $1/N_C$, while in the next-to-leading order analysis of the pion vector form factor $F_V = \sqrt{3}F$ is updated in Ref. [50], which has also been confirmed in the study of radiative tau decays [20] and the partial wave analysis of $\pi\pi$ scattering [51, 52]. Phenomenology determinations of $F_V = 147$ MeV and 180 MeV have been used in $\tau \rightarrow VP\nu_\tau$ [18] and $\tau \rightarrow K\bar{K}\pi$ [19] decays respectively. By estimating the pseudo-Goldstone decay constant at chiral limit by the pion decay constant F_π , one has

$$F_V = \sqrt{2}F = 131 \text{ MeV}, \quad F_V = \sqrt{3}F = 160 \text{ MeV}. \quad (35)$$

Apparently, a more precise value for F_V is needed in our discussion, since the physical processes we are discussing are mainly the radiative decays of vector resonances and precisely F_V describes the interaction of vector resonances and photon. Thus we decide to free F_V and fit its value in our program, in such a way we could predict a more reliable value, as F_V is rather sensitive to the processes we are considering. To exploit the high energy constraint for \tilde{c}_8 in Eq.(29), the value for the $U_A(1)$ anomaly mass M_0 is needed, which has been reviewed in Ref. [26] and also recently determined in Ref. [52]. We use the average value $M_0 = 900$ MeV from the two mentioned references throughout. For the other unmentioned inputs, unless an explicit statement is given, we will take the corresponding values from Ref. [12].

As advertised previously, although the main contribution of our current work is to determine the $\eta - \eta'$ mixing parameters in a more reliable theoretical framework, we include the relevant radiative processes without η and η' into our discussion as well. By performing the χ^2 fit, we can determine the unknown

resonance couplings and $\eta - \eta'$ mixing parameters:

$$\begin{aligned}
F_8 &= (1.37 \pm 0.07)F_\pi, & F_0 &= (1.19 \pm 0.18)F_\pi, \\
\theta_8 &= (-21.1 \pm 6.0)^\circ, & \theta_0 &= (-2.5 \pm 8.2)^\circ, \\
F_V &= (136.6 \pm 3.5)\text{MeV}, & \tilde{c}_3 &= 0.011 \pm 0.016, \\
\tilde{d}_2 &= 0.086 \pm 0.085, & \tilde{d}_5 &= 0.36 \pm 0.40,
\end{aligned} \tag{36}$$

with $\chi^2/\text{d.o.f} = 64.0/(70 - 8) = 1.03$. For the various decay widths, we summarize the experiment data and the results from our fitting program in Table 1 for the processes without η and η' and in Table 2 for those involving η or η' . To visualize the results, we plot the numbers in Tables 1 and 2 in Fig. 3, where one should notice we have scaled different decay widths to a proper range in order to show them in one figure. The resulting plots for the form factors of $\eta\gamma\gamma^*$, $\eta'\gamma\gamma^*$ and $\phi\eta\gamma^*$ are given in Figs. 4, 5 and 6, respectively. The error bands shown in the plots and the errors of the parameters in Eq. (36) correspond to the statistical uncertainties at 2 standard deviations [53]: $n_\sigma = (\chi^2 - \chi_0^2)/\sqrt{2\chi_0^2}$, with χ_0^2 the minimum χ^2 obtained in the fit and n_σ the number of standard deviations.

	Exp	Fit	Theo ($F_V = 160$ MeV)	Theo ($F_V = 180$ MeV)
$\Gamma_{\omega \rightarrow \pi\gamma}$	757 ± 28	731 ± 37	533	421
$\Gamma_{\rho^0 \rightarrow \pi^0\gamma}$	89.6 ± 12.6	76.0 ± 38	55.4	43.8
$\Gamma_{K^{*0} \rightarrow K^0\gamma}$	116 ± 12	113 ± 6	83	65
$\Gamma_{\omega \rightarrow \pi e^- e^+}$	6.54 ± 0.83	6.64 ± 0.33	4.84	3.83
$\Gamma_{\omega \rightarrow \pi\mu^- \mu^+}$	0.82 ± 0.21	0.66 ± 0.03	0.48	0.38

Table 1: Experimental and theoretical values of the various decay widths without η and η' . The experiment data are taken from [12]. All of the values are given in units of KeV unless specified. The results from our fit are listed in the column Fit and the error bands of the widths are calculated by using the same parameter configurations that we use to get the error bands for the parameters in Eq. (36). To show the relevance of F_V , we have given another two theoretical predictions for the various decay widths in the last two columns by taking $F_V = 160, 180$ MeV.

	Exp	Fit
$\Gamma_{\omega \rightarrow \eta\gamma}$	3.91 ± 0.38	5.05 ± 0.36
$\Gamma_{\rho^0 \rightarrow \eta\gamma}$	44.8 ± 3.5	41.6 ± 3.2
$\Gamma_{\phi \rightarrow \eta\gamma}$	55.6 ± 1.6	55.3 ± 2.5
$\Gamma_{\phi \rightarrow \eta'\gamma}$	0.265 ± 0.012	0.270 ± 0.021
$\Gamma_{\eta' \rightarrow \omega\gamma}$	6.2 ± 1.1	7.4 ± 1.0
$\Gamma_{\eta \rightarrow \gamma\gamma}$	0.510 ± 0.026	0.481 ± 0.038
$\Gamma_{\eta' \rightarrow \gamma\gamma}$	4.30 ± 0.15	4.25 ± 0.21
$\Gamma_{\eta \rightarrow \gamma e^- e^+}$	$(8.8 \pm 1.6) \times 10^{-3}$	$(8.0 \pm 0.6) \times 10^{-3}$
$\Gamma_{\eta \rightarrow \gamma \mu^- \mu^+}$	$(0.40 \pm 0.08) \times 10^{-3}$	$(0.38 \pm 0.03) \times 10^{-3}$
$\Gamma_{\eta' \rightarrow \gamma \mu^- \mu^+}$	$(2.1 \pm 0.7) \times 10^{-2}$	$(1.8 \pm 0.1) \times 10^{-2}$
$\Gamma_{\phi \rightarrow \eta e^- e^+}$	0.490 ± 0.048	0.464 ± 0.021

Table 2: Experimental and theoretical values of the various decay widths involving η and η' . The experiment data are taken from [12]. All of the values are given in units of KeV unless specified. The error bands of the widths are calculated by using the same parameter configurations as used in Table 1.

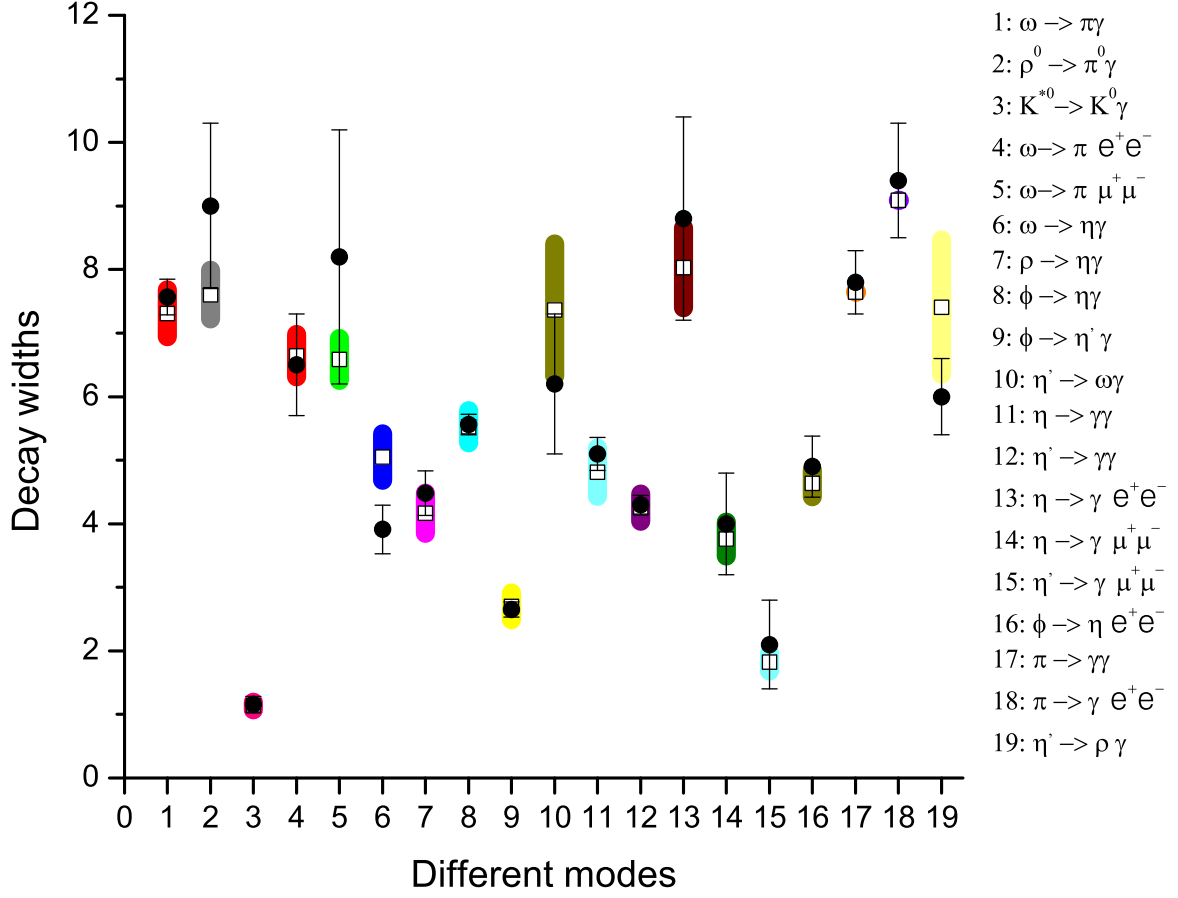


Figure 3: Different decay widths. We have scaled different decay widths into a common region in order to show them in one figure. For the values before scaling, see the numbers in Tables 1 and 2. The open squares denote the central values with the best fit given in Eq.(36), and the shaded area correspond to the error bands generated by the parameter configurations explained in the text after Eq.(36). Note that using the high energy constraints we can completely predict the decay widths of $\pi \rightarrow \gamma\gamma$ and $\pi \rightarrow \gamma e^+e^-$, which are in good agreement with the experimental data, and here we include these two processes just for completeness. We do not include $\eta' \rightarrow \rho\gamma$ in the fit, since PDG [12] also includes the background part from $\eta' \rightarrow \pi\pi\gamma$ to determine the width for $\eta' \rightarrow \rho\gamma$. Nevertheless due to the dominant decay channel of the ρ resonance is $\pi\pi$, our prediction for $\eta' \rightarrow \rho\gamma$ agrees with the one from PDG [12].

Several remarks about the fitting results are in order. We comment them as follows.

1. The first lesson we can learn from the results in Eq.(36) is that \tilde{c}_3 , \tilde{d}_2 and \tilde{d}_5 carry huge error bars. Nevertheless we find there exist strong correlations among these parameters. We plot the correlations of \tilde{d}_2 - \tilde{d}_5 , \tilde{c}_3 - \tilde{d}_2 and \tilde{c}_3 - \tilde{d}_5 respectively in Figs.(7), (8) and (9), where the same parameter configurations have been used as we exploit in evaluating the error bands in Eq.(36) and Figs.(4-6).

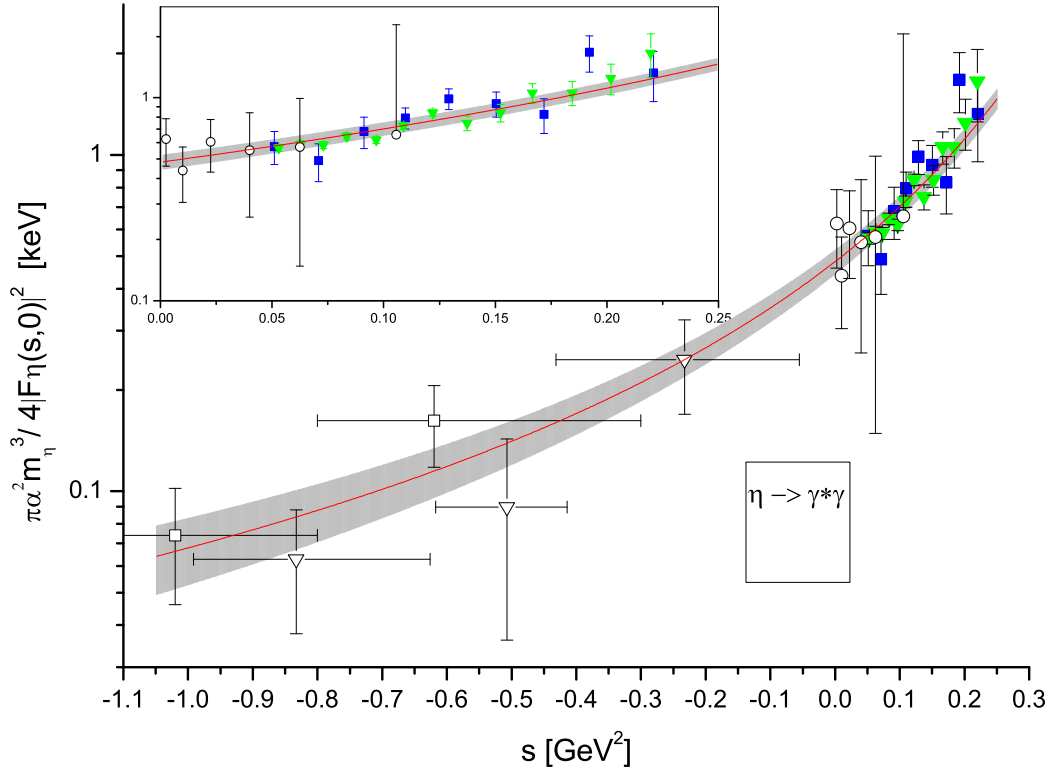


Figure 4: The form factors of $\eta \rightarrow \gamma^* \gamma$. The solid line (red) denotes the result from the best fit and the shaded area correspond to the error bands. Sources of the different experiment data are: solid squares [54, 55], open squares [56], open circles [57], solid triangles [58], open triangles [59]. The separated figure in the upper part is the close-up of the main plot in the region of $s > 0$.

A very strong linear correlation between \tilde{d}_2 and \tilde{d}_5 is observed, as one can see in Fig.(7). While the correlations of \tilde{c}_3 - \tilde{d}_2 and \tilde{c}_3 - \tilde{d}_5 , as shown in Figs.(8) and (9), are not as strong as \tilde{d}_2 - \tilde{d}_5 . A correlation between \tilde{c}_3 and \tilde{d}_2 (in fact they are c_3 and d_2 from the pseudo-Goldstone octet Lagrangian) has been revealed in a preliminary analysis of $\tau \rightarrow \pi \pi \eta \nu_\tau$ decay [61], where η particle is treated as the pure octet η_8 . The parameter space found in the previous reference covers most of the space shown in Fig. (8), but the correlation relation in [61] is with opposite sign of the relation we find in the present work. This indicates that the combining study of the radiative decay processes of η or η' and the τ decays involving η or η' may help us pin down the resonance parameters, such as \tilde{c}_3 and \tilde{d}_2 , which deserves a future work. For the remaining parameters in Eq.(36), we do not find significant correlations among them.

2. The value of F_V . As one can see in Eq.(36), our analysis favors a smaller value for F_V , comparing with the values used in [18] and [19]. By using the high energy constraints mentioned in previous section, the processes appearing in Table 1 are solely determined by F_V . Thus those radiative decay processes without η and η' provide a tight constraint on the value of F_V . To clearly show

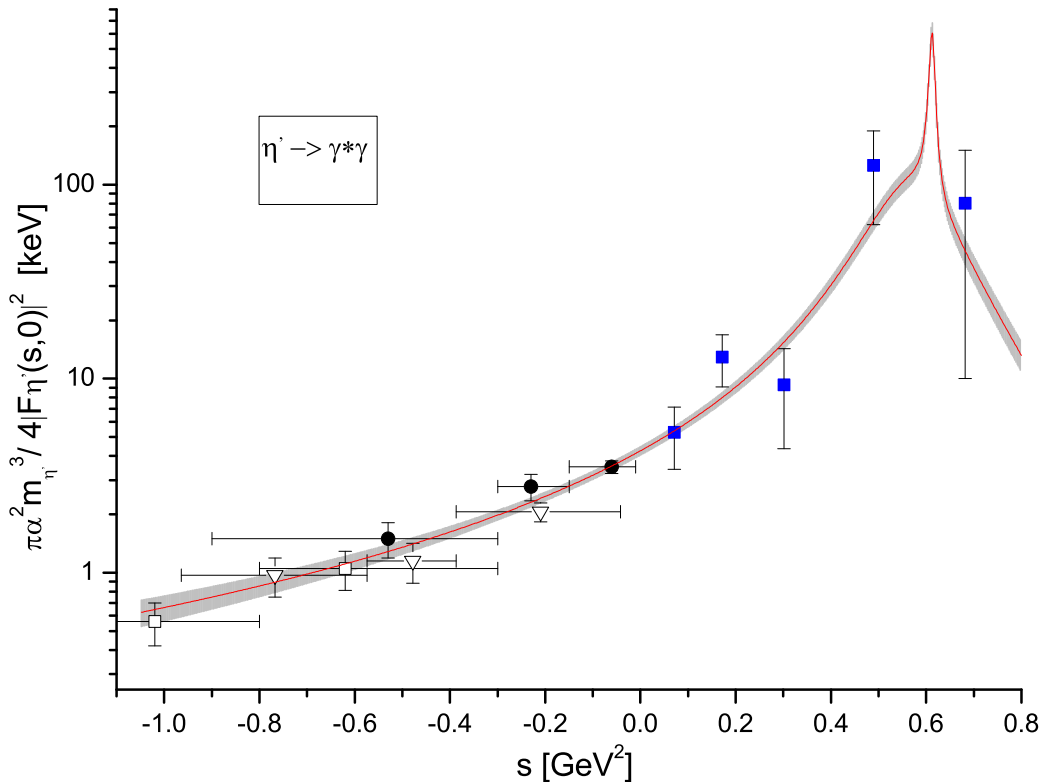


Figure 5: The form factors of $\eta' \rightarrow \gamma^* \gamma$. The solid line (red) denotes the result from the best fit and the shaded area correspond to the error bands. Sources of the different experiment data are: solid squares [54, 55], open squares [56], open triangles [59], solid circles [60].

the relevance of F_V in those channels, we give another two predictions by taking $F_V = 160$ and 180 MeV in the last two columns in Table 1. We also use these 5 processes in Table 1 to perform a fit to get the value of F_V , and the result is $F_V = (134.05 \pm 2.17)\text{MeV}$, with $\chi^2/\text{d.o.f} = \frac{1.46}{5-1} = 0.36$. This result for F_V is in perfect agreement with the global fit in Eq.(36). If one takes the value of $F_V = 134.05\text{MeV}$ and fits the other 7 unknown parameters by using the rest of experimental data as we used to get Eq.(36), the fit results turn out to be quite similar to the ones we show in Eq.(36), as expected.

3. The $\eta - \eta'$ mixing parameters. For F_8 , it can be completely fixed by the ratio of F_K/F_π in the next-to-next-to-leading order within the triple expansion of large N_C χPT , which yields a rather reliable prediction $F_8 = 1.34F_\pi$ [11]. However at the same order, there exist several unknown LECs for the predictions of F_0 and $\theta_0 - \theta_8$, which prevents the precise predictions for their values. As one can see in Eq.(36), our result for F_8 agrees with the χPT prediction. In Ref. [10], F_0 was determined in the process $P \rightarrow \gamma\gamma$ at next-to-leading order by ignoring the chiral symmetry breaking operators. Assuming OZI violating coupling in the next-to-leading order to vanish, $F_0 = 1.25F_\pi$ can be derived [10, 31]. F_0 can be also evaluated in the standard way to include the chiral corrections

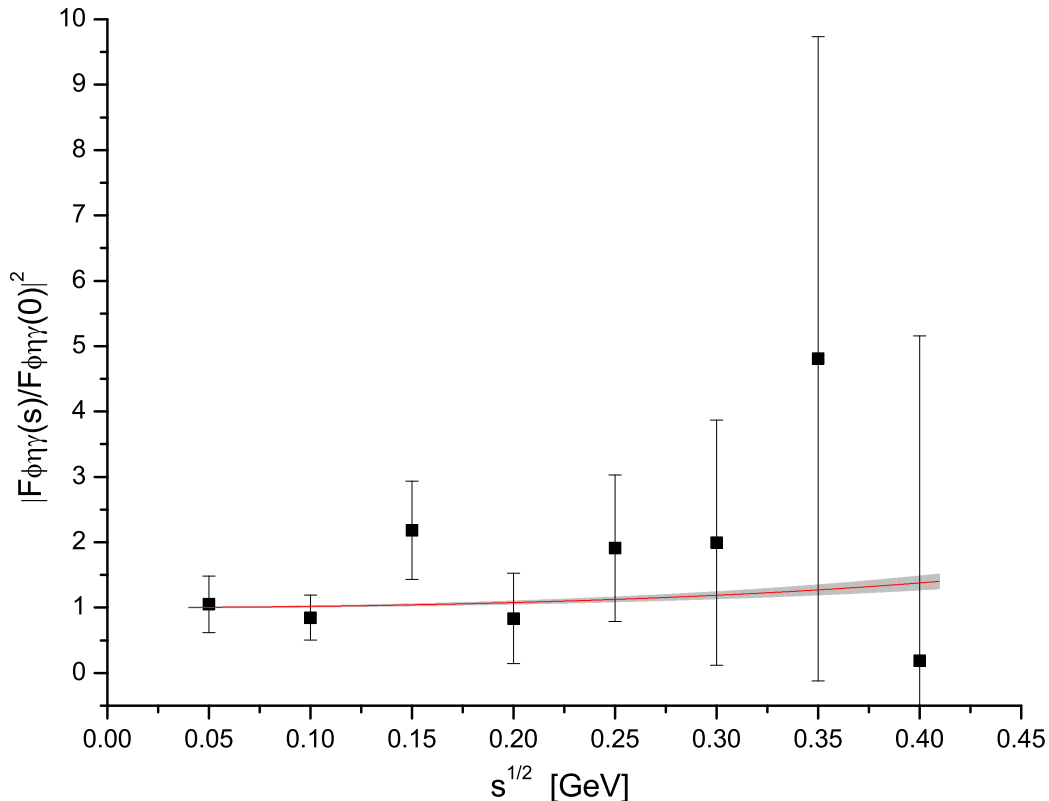


Figure 6: The form factors of $\phi \rightarrow \eta\gamma\gamma$ [57]. The solid line (red) denotes the result from the best fit and the shaded area correspond to the error bands.

from loops and LECs in the calculation of the axial-vector current matrix element [11]. In this case, two additional OZI violating couplings appear and if one assumes those couplings to vanish, $F_0 \simeq F_\pi$ can be predicted. So a reliable determination of F_0 could help us better understand the somewhat inconsistent results from the two approaches. As an improvement, we have included not only the OZI violating operators but also the chiral symmetry breaking ones in $R\chi T$ to determine the value of F_0 in $P \rightarrow \gamma\gamma$ processes. Our result shows the inclusion of the OZI suppressed and higher chiral symmetry breaking operators in the calculation of $P \rightarrow \gamma\gamma$ does not change the result of $F_0 = 1.25F_\pi$ very much, as obtained in [10]. This also indicates that the ignorance of the OZI suppressed operators in the calculation of the axial-vector current matrix element, which leads to $F_0 \simeq F_\pi$, is not a good approximation. About the mixing angles, our result $\theta_8 = (-21.1 \pm 6.0)^\circ$ agrees well with the results in literature, see Table 1 of Ref. [26]. While for the mixing angle θ_0 , our analysis reveals that a huge error accompanies this parameter, as shown in Eq.(36). This may be viewed as a source that why rather different results have been obtained for θ_0 [26].

By using simple parameterizations of the $VP\gamma$ and $P\gamma\gamma$ vertexes that only consist of constant terms (independent of the quark masses and momenta), the $\eta - \eta'$ mixing parameters have been explored

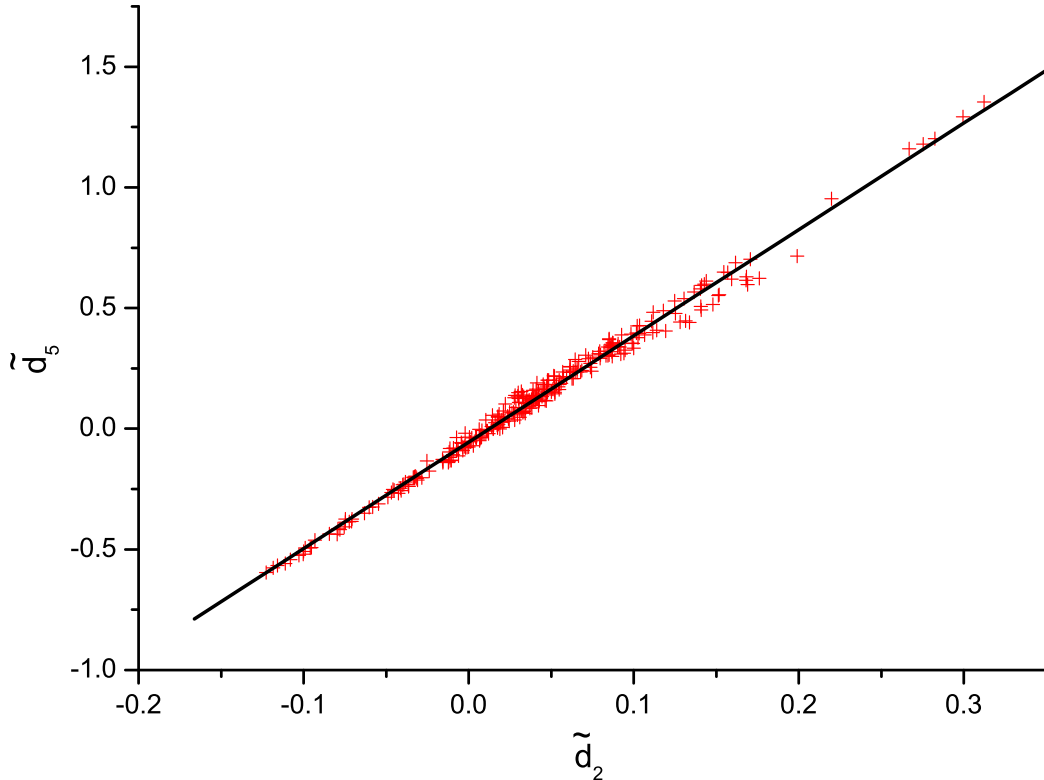


Figure 7: The correlations between \tilde{d}_2 and \tilde{d}_5 . The solid line (black) corresponds to $\tilde{d}_5 = 4.4\tilde{d}_2 - 0.06$.

in various $V \rightarrow P\gamma$ and $P \rightarrow \gamma\gamma$ processes and one can see Ref. [26] for a comprehensive analysis of different results. Our current work confirms the validity of the two-mixing-angle description in a more general framework for $VP\gamma$ and $P\gamma\gamma$ interaction vertexes. Within the current theoretical framework, the various data from different radiative decay processes can be simultaneously incorporated and our χ^2 is clearly better than that in Ref. [38].

4. An additional interest of our work is to test the resonance saturation assumption for the couplings relevant to the chiral anomaly induced processes $P \rightarrow \gamma\gamma$, with $P = \pi, \eta, \eta'$. The next-to-leading order odd intrinsic parity operators in the chiral Lagrangian with only pseudo Goldstone bosons can be categorized into two parts: $O(N_C^1 p^6)$ and $O(N_C^0 p^4)$ [21, 62]:

$$\tilde{L}_{odd}^{(2)} = i\tilde{t}_1 \varepsilon_{\mu\nu\alpha\beta} \langle \tilde{\chi}_- \tilde{f}_+^{\mu\nu} \tilde{f}_+^{\alpha\beta} \rangle - \tilde{t}_2 \varepsilon_{\mu\nu\alpha\beta} \langle \nabla_\lambda f_+^{\lambda\mu} \{ f_+^{\alpha\beta}, u^\nu \} \rangle + \tilde{k}_3 \varepsilon_{\mu\nu\alpha\beta} \langle \tilde{f}_+^{\mu\nu} \tilde{f}_+^{\alpha\beta} \rangle \sqrt{6} \tilde{\phi}_0. \quad (37)$$

The higher order LECs appearing in the pseudo-Goldstone chiral Lagrangian encode the high energy dynamics of the underlying theory. In the resonance saturation approach, it is assumed that the high order LECs are completely saturated by the resonances and thus one does not need to include extra pure higher order pseudo-Goldstone operators in the resonance Lagrangian. This assumption has been proven to be very successful for the $O(p^4)$ χ PT LECs in the even intrinsic parity sector [14]. In the present discussion, we shall check this assumption in the odd intrinsic parity sector. By

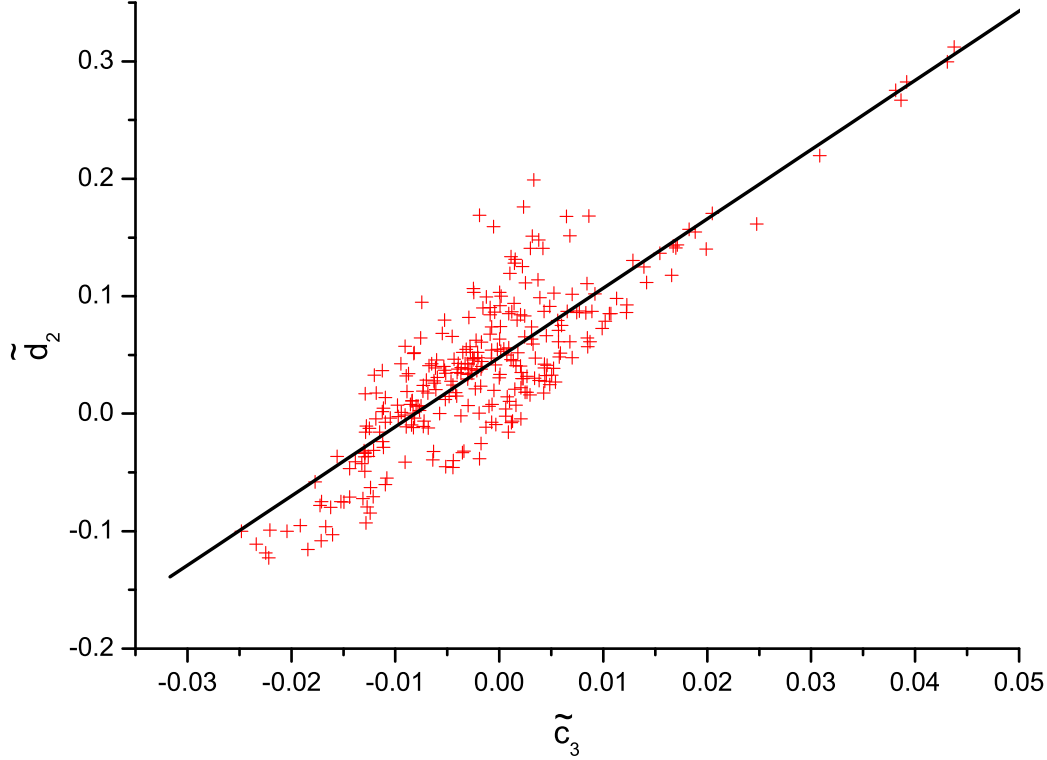


Figure 8: The correlations between \tilde{c}_3 and \tilde{d}_2 . The solid line (black) corresponds to $\tilde{d}_2 = 5.6\tilde{c}_3 + 0.06$.

integrating out the vector resonances in the resonance chiral Lagrangian introduced in Sect. 3, we have the following predictions

$$\tilde{t}_1^V = -\frac{F_V}{4\sqrt{2}M_V^3}(\tilde{c}_1 + \tilde{c}_2 + 8\tilde{c}_3 - \tilde{c}_5) + \frac{F_V^2}{8M_V^4}(\tilde{d}_1 + 8\tilde{d}_2 - \tilde{d}_3), \quad (38)$$

$$\tilde{t}_2^V = -\frac{F_V}{\sqrt{2}M_V^3}(\tilde{c}_5 - \tilde{c}_6) + \frac{F_V^2}{2M_V^4}\tilde{d}_3, \quad (39)$$

$$\tilde{k}_3 = -\frac{F_V M_0^2}{6\sqrt{2}M_V^3}(\tilde{c}_1 + \tilde{c}_2 - \tilde{c}_5) - \frac{F_V \tilde{c}_8}{2\sqrt{3}M_V} + \frac{F_V^2 M_0^2}{12M_V^4}(\tilde{d}_1 - \tilde{d}_3) + \frac{F_V^2 \tilde{d}_5}{2\sqrt{6}M_V^2}, \quad (40)$$

where $\tilde{t}_1^V, \tilde{t}_2^V$ coincide with the results in Ref. [25] and the result for \tilde{k}_3 is a new result to our knowledge. Taking into account the high energy constraints of the resonance couplings in Eqs.(24)(27)(29) and (33), we have the simplified predictions

$$\tilde{t}_1^V = \frac{F^2}{64M_V^4}, \quad \tilde{t}_2^V = -\frac{N_C}{64\pi^2 M_V^2}, \quad \tilde{k}_3^V = \frac{F^2 M_0^2}{96M_V^4} - \frac{2F_V^2 M_0^2}{3M_V^4}\tilde{d}_2 + \frac{F_V^2}{2\sqrt{6}M_V^2}\tilde{d}_5, \quad (41)$$

The fitted results in Eq.(36) yield

$$\tilde{t}_1 = 0.37 \times 10^{-3} \text{ GeV}^{-2}, \quad \tilde{t}_2 = -8.0 \times 10^{-3} \text{ GeV}^{-2}, \quad \tilde{k}_3 = (0.83 \pm 3.02) \times 10^{-4}, \quad (42)$$

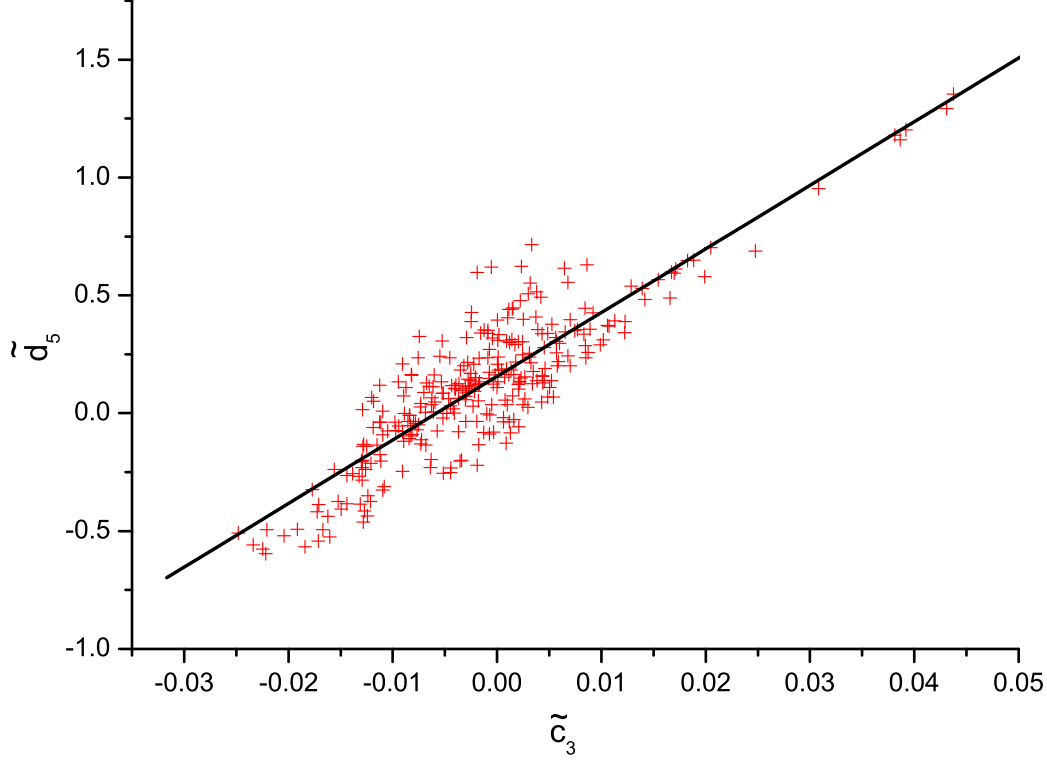


Figure 9: The correlations between \tilde{c}_3 and \tilde{d}_5 . The solid line (black) corresponds to $\tilde{d}_5 = 25\tilde{c}_3 + 0.2$.

where the error of k_3 is estimated by taking the errors from the fit results in Eq.(36).

Now we can calculate the form factors of $P \rightarrow \gamma\gamma$ using the pseudo-Goldstone Lagrangian in Eq.(5) and Eq.(37). For $\pi \rightarrow \gamma\gamma$, the k_3 operator is irrelevant and our result is the same as the one in Ref. [25]

$$F_{\pi \rightarrow \gamma\gamma} = F_{\pi \rightarrow \gamma\gamma}^{\text{WZW}} + F_{\pi \rightarrow \gamma\gamma}^{\tilde{t}_1}, \quad (43)$$

where $F_{\pi \rightarrow \gamma\gamma}^{\text{WZW}}$ denotes the contribution from the WZW Lagrangian in Eq.(5)

$$F_{\pi \rightarrow \gamma\gamma}^{\text{WZW}} = -\frac{1}{4\pi^2 F_\pi}, \quad (44)$$

and $F_{\pi \rightarrow \gamma\gamma}^{\tilde{t}_1}$ denotes the contribution from the \tilde{t}_1 term

$$F_{\pi \rightarrow \gamma\gamma}^{\tilde{t}_1} = \frac{64}{3F_\pi} m_\pi^2 \tilde{t}_1. \quad (45)$$

Note that the \tilde{t}_2 operator does not contribute to the considered process. For $\eta \rightarrow \gamma\gamma$, we have

$$F_{\eta \rightarrow \gamma\gamma} = F_{\eta \rightarrow \gamma\gamma}^{\text{WZW}} + F_{\eta \rightarrow \gamma\gamma}^{\tilde{t}_1} + F_{\eta \rightarrow \gamma\gamma}^{\tilde{k}_3}, \quad (46)$$

where

$$F_{\eta \rightarrow \gamma\gamma}^{\text{WZW}} = -\frac{1}{\cos(\theta_0 - \theta_8)} \frac{1}{4\sqrt{3}\pi^2} \left(\frac{\cos \theta_0}{F_8} - \frac{\sqrt{8} \sin \theta_8}{F_0} \right), \quad (47)$$

and $F_{\eta \rightarrow \gamma\gamma}^{\tilde{t}_1}$, $F_{\eta \rightarrow \gamma\gamma}^{\tilde{k}_3}$ denote the contributions from \tilde{t}_1, \tilde{k}_3 operators respectively

$$F_{\eta \rightarrow \gamma\gamma}^{\tilde{t}_1} = \frac{1}{\cos(\theta_0 - \theta_8)} \left\{ \frac{64}{9\sqrt{3}} (7m_\pi^2 - 4m_K^2) \frac{\cos \theta_0}{F_8} + \frac{128\sqrt{2}}{9\sqrt{3}} (2m_\pi^2 + m_K^2) \frac{-\sin \theta_8}{F_0} \right\} \tilde{t}_1, \quad (48)$$

$$F_{\eta \rightarrow \gamma\gamma}^{\tilde{k}_3} = -\frac{1}{\cos(\theta_0 - \theta_8)} \frac{64\sqrt{6} \sin \theta_8}{3F_0} \tilde{k}_3. \quad (49)$$

Similar result for $\eta' \rightarrow \gamma\gamma$ is found to be

$$F_{\eta' \rightarrow \gamma\gamma} = F_{\eta' \rightarrow \gamma\gamma}^{\text{WZW}} + F_{\eta' \rightarrow \gamma\gamma}^{\tilde{t}_1} + F_{\eta' \rightarrow \gamma\gamma}^{\tilde{k}_3}, \quad (50)$$

where

$$F_{\eta' \rightarrow \gamma\gamma}^{\text{WZW}} = -\frac{1}{\cos(\theta_0 - \theta_8)} \frac{1}{4\sqrt{3}\pi^2} \left(\frac{\sin \theta_0}{F_8} + \frac{\sqrt{8} \cos \theta_8}{F_0} \right), \quad (51)$$

$$F_{\eta' \rightarrow \gamma\gamma}^{\tilde{t}_1} = \frac{1}{\cos(\theta_0 - \theta_8)} \left\{ \frac{64}{9\sqrt{3}} (7m_\pi^2 - 4m_K^2) \frac{\sin \theta_0}{F_8} + \frac{128\sqrt{2}}{9\sqrt{3}} (2m_\pi^2 + m_K^2) \frac{\cos \theta_8}{F_0} \right\} \tilde{t}_1, \quad (52)$$

$$F_{\eta' \rightarrow \gamma\gamma}^{\tilde{k}_3} = \frac{1}{\cos(\theta_0 - \theta_8)} \frac{64\sqrt{6} \cos \theta_8}{3F_0} \tilde{k}_3. \quad (53)$$

In Table 3, we show different contributions to the form factor $F_{P \rightarrow \gamma\gamma}$ using the predictions for \tilde{t}_1 and \tilde{k}_3 in Eq.(42). For the $\pi \rightarrow \gamma\gamma$ process, the chiral symmetry breaking effect is rather tiny, about 1%, since the chiral correction is proportional to m_π^2/M_V^2 . Hence the leading order contribution from the WZW Lagrangian overwhelmingly dominates the decay width of $\pi \rightarrow \gamma\gamma$ [25, 36]. For $\eta \rightarrow \gamma\gamma$ and $\eta' \rightarrow \gamma\gamma$, the WZW term can also give rather close results to the experimental values, as one can see in Table 3 the next-to-leading order correction is only at most 14% of the WZW term. So our current calculations confirm the validity of the triple expansion scheme for the odd intrinsic parity pseudo-Goldstone Lagrangian, i.e. the WZW contribution plays the dominant role in the $P \rightarrow \gamma\gamma$ processes. We point out that this conclusion is based on the fact we have used the fitted results for the mixing parameters in Eq.(36).

	$F_{P \rightarrow \gamma\gamma}^{\text{WZW}}$	$F_{P \rightarrow \gamma\gamma}^{\tilde{t}_1}$	$F_{P \rightarrow \gamma\gamma}^{\tilde{k}_3}$	$F_{P \rightarrow \gamma\gamma}^{\text{WZW}+\tilde{t}_1+\tilde{k}_3}$	$F_{P \rightarrow \gamma\gamma}^{\text{EX}}$
$\pi \rightarrow \gamma\gamma$	-0.274	0.002	0	-0.272	-0.275 ± 0.070
$\eta \rightarrow \gamma\gamma$	-0.265	-0.007	0.015	-0.256	-0.272 ± 0.070
$\eta' \rightarrow \gamma\gamma$	-0.365	0.011	0.039	-0.315	-0.342 ± 0.012

Table 3: The predictions of different contributions to the form factors $F_{P \rightarrow \gamma\gamma}$ using the parameter values in Eq.(42). All of the values are given in units of GeV^{-1} .

5. We can predict the decay widths of $\rho \rightarrow \pi e^+ e^-$, $\eta' \rightarrow \gamma e^+ e^-$ and $\phi \rightarrow \eta \mu^+ \mu^-$ by using the results from the global fit Eq.(36):

$$\begin{aligned}\Gamma_{\rho \rightarrow \pi e^+ e^-} &= (3.42 \pm 0.17) \times 10^{-1} \text{KeV}, & \Gamma_{\eta' \rightarrow \gamma e^+ e^-} &= (8.85 \pm 0.48) \times 10^{-2} \text{KeV} \\ \Gamma_{\phi \rightarrow \eta \mu^+ \mu^-} &= (2.22 \pm 0.13) \times 10^{-2} \text{KeV},\end{aligned}\quad (54)$$

These predictions are below the upper limits given in PDG [12]. Hence our results can provide a theoretical hint to the future experimental analysis on these channels.

7 Conclusion

In this work, we complete the resonance chiral Lagrangian in the odd intrinsic parity sector (VVP type) by including the singlet η_1 field as the dynamical degree of freedom. We exploit this Lagrangian to study radiative decay processes: $P \rightarrow V\gamma$, $V \rightarrow P\gamma$, $P \rightarrow \gamma\gamma$, $P \rightarrow \gamma l^+ l^-$, $V \rightarrow Pl^+ l^-$, as well as the form factors of $\eta \rightarrow \gamma\gamma^*$, $\eta' \rightarrow \gamma\gamma^*$, $\phi \rightarrow \eta\gamma^*$. The two-mixing-angle scheme is used to describe the $\eta - \eta'$ system in the discussion. By imposing the proper short distance behavior of QCD, we can fix several combinations of the unknown resonance couplings. The remaining free resonance parameters, together with the mixing parameters $F_8, F_0, \theta_8, \theta_0$ are determined through fitting the various experimental data. We have shown the resonance chiral Lagrangian can provide a systematic theoretical framework to handle the various radiative decay processes involving the resonance states and simultaneously accommodate the various experimental data. Thus we believe the $\eta - \eta'$ mixing parameters resulted from this analysis should be rather reliable.

By integrating out the resonance states in R χ T, we predict the higher order low energy constants in the odd intrinsic parity pseudo-Goldstone Lagrangian. We conclude the WZW contribution from the leading order dominates the processes of $P \rightarrow \gamma\gamma$, with $P = \pi, \eta$ and η' , by using the $\eta - \eta'$ mixing parameters from our current analysis. We have also predicted the decay widths of $\rho \rightarrow \pi e^+ e^-$, $\eta' \rightarrow \gamma e^+ e^-$ and $\phi \rightarrow \eta \mu^+ \mu^-$, which may shed light on the future measurement for these three channels.

Acknowledgments

We thank Jose Antonio Oller and Juan Jose Sanz-Cillero for discussions. This work is supported in part by National Nature Science Foundations of China under contract numbers 10925522, 10875001, 11021092 and 11105038. ZHG also acknowledges the grants from Natural Science Foundation of Hebei Province with contract number A2011205093, Doctor Foundation of Hebei Normal University with contract number L2010B04, MEC FPA2010-17806 and the Consolider-Ingenio 2010 Programme CPAN (CSD2007-00042).

A The decay widths of $V \rightarrow P\gamma$, $P \rightarrow V\gamma$ and $P \rightarrow \gamma\gamma$

The various decay widths from different processes are given below

$$\begin{aligned}\Gamma(\omega \rightarrow \pi\gamma) &= \frac{1}{3} \alpha \left(\frac{M_\omega^2 - m_\pi^2}{2M_\omega} \right)^3 \\ &\left\{ - \frac{2\sqrt{2}}{F_\pi M_V M_\omega} [(\tilde{c}_1 + \tilde{c}_2 + 8\tilde{c}_3 - \tilde{c}_5)m_\pi^2 + (\tilde{c}_2 + \tilde{c}_5 - \tilde{c}_1 - 2\tilde{c}_6)M_\omega^2] \right. \\ &\quad \left. + \frac{4F_V}{F_\pi M_\omega M_\rho^2} [(\tilde{d}_1 + 8\tilde{d}_2 - \tilde{d}_3)m_\pi^2 + \tilde{d}_3 M_\omega^2] \right\}^2,\end{aligned}\quad (55)$$

$$\begin{aligned}
\Gamma(\rho^0 \rightarrow \pi^0 \gamma) &= \frac{1}{3} \alpha \left(\frac{M_\rho^2 - m_\pi^2}{2M_\rho} \right)^3 \\
&\left\{ -\frac{2\sqrt{2}}{3F_\pi M_V M_\rho} [(\tilde{c}_1 + \tilde{c}_2 + 8\tilde{c}_3 - \tilde{c}_5)m_\pi^2 + (\tilde{c}_2 + \tilde{c}_5 - \tilde{c}_1 - 2\tilde{c}_6)M_\rho^2] \right. \\
&\quad \left. + \frac{4F_V}{3F_\pi M_\rho M_\omega^2} [(\tilde{d}_1 + 8\tilde{d}_2 - \tilde{d}_3)m_\pi^2 + \tilde{d}_3 M_\rho^2] \right\}^2, \tag{56}
\end{aligned}$$

$$\begin{aligned}
\Gamma(K^{*0} \rightarrow K^0 \gamma) &= \frac{1}{3} \alpha \left(\frac{M_{K^*}^2 - m_K^2}{2M_{K^*}} \right)^3 \\
&\left\{ \frac{4\sqrt{2}}{3F_\pi M_V M_{K^*}} [(\tilde{c}_1 + \tilde{c}_2 + 8\tilde{c}_3 - \tilde{c}_5)m_K^2 + (\tilde{c}_2 + \tilde{c}_5 - \tilde{c}_1 - 2\tilde{c}_6)M_{K^*}^2] \right. \\
&\quad \left. + \frac{2F_V}{3F_\pi M_{K^*}} \left(\frac{1}{M_\omega^2} - \frac{3}{M_\rho^2} - \frac{2}{M_\phi^2} \right) [(\tilde{d}_1 + 8\tilde{d}_2 - \tilde{d}_3)m_K^2 + \tilde{d}_3 M_{K^*}^2] \right\}^2, \tag{57}
\end{aligned}$$

$$\begin{aligned}
\Gamma(\rho \rightarrow \eta \gamma) &= \frac{1}{3} \alpha \left(\frac{M_\rho^2 - m_\eta^2}{2M_\rho} \right)^3 \frac{1}{\cos(\theta_0 - \theta_8)^2} \left\{ \right. \\
&\quad -\frac{2\sqrt{2}}{\sqrt{3}M_V M_\rho} \left(\frac{\cos \theta_0}{F_8} - \frac{\sqrt{2} \sin \theta_8}{F_0} \right) [M_\rho^2(\tilde{c}_2 - \tilde{c}_1 + \tilde{c}_5 - 2\tilde{c}_6) + m_\eta^2(\tilde{c}_2 + \tilde{c}_1 - \tilde{c}_5) + 8\tilde{c}_3 m_\pi^2] \\
&\quad + \frac{4F_V}{\sqrt{3}M_\rho^3} \left(\frac{\cos \theta_0}{F_8} - \frac{\sqrt{2} \sin \theta_8}{F_0} \right) [\tilde{d}_3(M_\rho^2 - m_\eta^2) + \tilde{d}_1 m_\eta^2 + 8\tilde{d}_2 m_\pi^2] \\
&\quad \left. + \left(-\frac{\sin \theta_8}{F_0} \right) \left[-\frac{4\sqrt{2}M_V}{M_\rho} \tilde{c}_8 + \frac{8F_V M_V^2}{M_\rho^3} \tilde{d}_5 \right] \right\}^2, \tag{58}
\end{aligned}$$

$$\begin{aligned}
\Gamma(\omega \rightarrow \eta \gamma) &= \frac{1}{9} \Gamma_{\rho \rightarrow \eta \gamma} [M_\rho \rightarrow M_\omega] \\
&= \frac{1}{27} \alpha \left(\frac{M_\omega^2 - m_\eta^2}{2M_\omega} \right)^3 \frac{1}{\cos(\theta_0 - \theta_8)^2} \left\{ \right. \\
&\quad -\frac{2\sqrt{2}}{\sqrt{3}M_V M_\omega} \left(\frac{\cos \theta_0}{F_8} - \frac{\sqrt{2} \sin \theta_8}{F_0} \right) [M_\omega^2(\tilde{c}_2 - \tilde{c}_1 + \tilde{c}_5 - 2\tilde{c}_6) + m_\eta^2(\tilde{c}_2 + \tilde{c}_1 - \tilde{c}_5) + 8\tilde{c}_3 m_\pi^2] \\
&\quad + \frac{4F_V}{\sqrt{3}M_\omega^3} \left(\frac{\cos \theta_0}{F_8} - \frac{\sqrt{2} \sin \theta_8}{F_0} \right) [\tilde{d}_3(M_\omega^2 - m_\eta^2) + \tilde{d}_1 m_\eta^2 + 8\tilde{d}_2 m_\pi^2] \\
&\quad \left. + \left(-\frac{\sin \theta_8}{F_0} \right) \left[-\frac{4\sqrt{2}M_V}{M_\omega} \tilde{c}_8 + \frac{8F_V M_V^2}{M_\omega^3} \tilde{d}_5 \right] \right\}^2, \tag{59}
\end{aligned}$$

$$\begin{aligned}
\Gamma(\phi \rightarrow \eta\gamma) &= \frac{1}{3}\alpha\left(\frac{M_\phi^2 - m_\eta^2}{2M_\phi}\right)^3 \frac{1}{\cos(\theta_0 - \theta_8)^2} \left\{ \right. \\
&\quad \frac{4\sqrt{2}}{3\sqrt{3}M_V M_\phi} \times \\
&\quad \times \left(\frac{\sqrt{2}\cos\theta_0}{F_8} + \frac{\sin\theta_8}{F_0}\right) [M_\phi^2(\tilde{c}_2 - \tilde{c}_1 + \tilde{c}_5 - 2\tilde{c}_6) + m_\eta^2(\tilde{c}_2 + \tilde{c}_1 - \tilde{c}_5) + 8\tilde{c}_3(2m_K^2 - m_\pi^2)] \\
&\quad - \frac{8F_V}{3\sqrt{3}M_\phi^3} \left(\frac{\sqrt{2}\cos\theta_0}{F_8} + \frac{\sin\theta_8}{F_0}\right) [\tilde{d}_3(M_\phi^2 - m_\eta^2) + \tilde{d}_1 m_\eta^2 + 8\tilde{d}_2(2m_K^2 - m_\pi^2)] \\
&\quad \left. + \left(-\frac{\sin\theta_8}{F_0}\right) \left[-\frac{8M_V}{3M_\phi}\tilde{c}_8 + \frac{8\sqrt{2}F_V M_V^2}{3M_\phi^3}\tilde{d}_5\right] \right\}^2, \tag{60}
\end{aligned}$$

$$\begin{aligned}
\Gamma(\phi \rightarrow \eta'\gamma) &= \frac{1}{3}\alpha\left(\frac{M_\phi^2 - m_{\eta'}^2}{2M_\phi}\right)^3 \frac{1}{\cos(\theta_0 - \theta_8)^2} \left\{ \right. \\
&\quad \frac{4\sqrt{2}}{3\sqrt{3}M_V M_\phi} \times \\
&\quad \times \left(\frac{\sqrt{2}\sin\theta_0}{F_8} - \frac{\cos\theta_8}{F_0}\right) [M_\phi^2(\tilde{c}_2 - \tilde{c}_1 + \tilde{c}_5 - 2\tilde{c}_6) + m_{\eta'}^2(\tilde{c}_2 + \tilde{c}_1 - \tilde{c}_5) + 8\tilde{c}_3(2m_K^2 - m_\pi^2)] \\
&\quad - \frac{8F_V}{3\sqrt{3}M_\phi^3} \left(\frac{\sqrt{2}\sin\theta_0}{F_8} - \frac{\cos\theta_8}{F_0}\right) [\tilde{d}_3(M_\phi^2 - m_{\eta'}^2) + \tilde{d}_1 m_{\eta'}^2 + 8\tilde{d}_2(2m_K^2 - m_\pi^2)] \\
&\quad \left. + \left(\frac{\cos\theta_8}{F_0}\right) \left[-\frac{8M_V}{3M_\phi}\tilde{c}_8 + \frac{8\sqrt{2}F_V M_V^2}{3M_\phi^3}\tilde{d}_5\right] \right\}^2, \tag{61}
\end{aligned}$$

$$\begin{aligned}
\Gamma(\eta' \rightarrow \omega\gamma) &= \frac{1}{9}\Gamma_{\eta' \rightarrow \rho\gamma}[M_\rho \rightarrow M_\omega] \\
&= \frac{1}{9}\alpha\left(\frac{m_{\eta'}^2 - M_\omega^2}{2m_{\eta'}}\right)^3 \frac{1}{\cos(\theta_0 - \theta_8)^2} \left\{ \right. \\
&\quad \frac{2\sqrt{2}}{\sqrt{3}M_V M_\omega} \left(\frac{\sin\theta_0}{F_8} + \frac{\sqrt{2}\cos\theta_8}{F_0}\right) [M_\omega^2(\tilde{c}_2 - \tilde{c}_1 + \tilde{c}_5 - 2\tilde{c}_6) + m_{\eta'}^2(\tilde{c}_2 + \tilde{c}_1 - \tilde{c}_5) + 8\tilde{c}_3 m_\pi^2] \\
&\quad - \frac{4F_V}{\sqrt{3}M_\omega^3} \left(\frac{\sin\theta_0}{F_8} + \frac{\sqrt{2}\cos\theta_8}{F_0}\right) [\tilde{d}_3(M_\omega^2 - m_{\eta'}^2) + \tilde{d}_1 m_{\eta'}^2 + 8\tilde{d}_2 m_\pi^2] \\
&\quad \left. + \left(\frac{\cos\theta_8}{F_0}\right) \left[\frac{4\sqrt{2}M_V}{M_\omega}\tilde{c}_8 - \frac{8F_V M_V^2}{M_\omega^3}\tilde{d}_5\right] \right\}^2, \tag{62}
\end{aligned}$$

$$\begin{aligned}
\Gamma(\pi \rightarrow \gamma\gamma) &= \frac{1}{4}\pi\alpha^2 M_\pi^3 \\
&\quad \left\{ -\frac{N_C}{12\pi^2 F_\pi} - \frac{4\sqrt{2}F_V}{3F_\pi M_V} \left(\frac{1}{M_\rho^2} + \frac{1}{M_\omega^2}\right) (\tilde{c}_1 + \tilde{c}_2 + 8\tilde{c}_3 - \tilde{c}_5) m_\pi^2 \right. \\
&\quad \left. + \frac{8F_V^2}{3F_\pi} \left(\frac{1}{M_\rho^2 M_\omega^2}\right) (\tilde{d}_1 + 8\tilde{d}_2 - \tilde{d}_3) m_\pi^2 \right\}^2, \tag{63}
\end{aligned}$$

$$\begin{aligned}
\Gamma(\eta \rightarrow \gamma\gamma) &= \frac{1}{4}\pi\alpha^2 M_\eta^3 \frac{1}{\cos(\theta_0 - \theta_8)^2} \left\{ -\frac{N_C}{12\sqrt{3}\pi^2} \left(\frac{\cos\theta_0}{F_8} - \frac{2\sqrt{2}\sin\theta_8}{F_0} \right) \right. \\
&- \frac{4\sqrt{2}F_V}{\sqrt{3}M_V} \left(\frac{1}{M_\rho^2} + \frac{1}{9M_\omega^2} \right) [m_\eta^2(\tilde{c}_2 + \tilde{c}_1 - \tilde{c}_5) + 8\tilde{c}_3 m_\pi^2] \left(\frac{\cos\theta_0}{F_8} - \frac{\sqrt{2}\sin\theta_8}{F_0} \right) \\
&+ \frac{16F_V}{9\sqrt{3}M_V} \left(\frac{1}{M_\phi^2} \right) [m_\eta^2(\tilde{c}_2 + \tilde{c}_1 - \tilde{c}_5) + 8\tilde{c}_3(2m_K^2 - m_\pi^2)] \left(\frac{\sqrt{2}\cos\theta_0}{F_8} + \frac{\sin\theta_8}{F_0} \right) \\
&+ \frac{4F_V^2}{\sqrt{3}} \left(\frac{1}{M_\rho^4} + \frac{1}{9M_\omega^4} \right) [\tilde{d}_1 m_\eta^2 - \tilde{d}_3 m_\eta^2 + 8\tilde{d}_2 m_\pi^2] \left(\frac{\cos\theta_0}{F_8} - \frac{\sqrt{2}\sin\theta_8}{F_0} \right) \\
&- \frac{8\sqrt{2}F_V^2}{9\sqrt{3}} \left(\frac{1}{M_\phi^4} \right) [\tilde{d}_1 m_\eta^2 - \tilde{d}_3 m_\eta^2 + 8\tilde{d}_2(2m_K^2 - m_\pi^2)] \left(\frac{\sqrt{2}\cos\theta_0}{F_8} + \frac{\sin\theta_8}{F_0} \right) \\
&+ \left(-\frac{\sin\theta_8}{F_0} \right) \left[-8\sqrt{2}M_V F_V \tilde{c}_8 \left(\frac{1}{M_\rho^2} + \frac{1}{9M_\omega^2} + \frac{2}{9M_\phi^2} \right) \right. \\
&\quad \left. + 8F_V^2 M_V^2 \tilde{d}_5 \left(\frac{1}{M_\rho^4} + \frac{1}{9M_\omega^4} + \frac{2}{9M_\phi^4} \right) \right] \Big\}^2, \tag{64}
\end{aligned}$$

$$\begin{aligned}
\Gamma(\eta' \rightarrow \gamma\gamma) &= \frac{1}{4}\pi\alpha^2 M_{\eta'}^3 \frac{1}{\cos(\theta_0 - \theta_8)^2} \left\{ -\frac{N_C}{12\sqrt{3}\pi^2} \left(\frac{\sin\theta_0}{F_8} + \frac{2\sqrt{2}\cos\theta_8}{F_0} \right) \right. \\
&- \frac{4\sqrt{2}F_V}{\sqrt{3}M_V} \left(\frac{1}{M_\rho^2} + \frac{1}{9M_\omega^2} \right) [m_{\eta'}^2(\tilde{c}_2 + \tilde{c}_1 - \tilde{c}_5) + 8\tilde{c}_3 m_\pi^2] \left(\frac{\sin\theta_0}{F_8} + \frac{\sqrt{2}\cos\theta_8}{F_0} \right) \\
&+ \frac{16F_V}{9\sqrt{3}M_V} \left(\frac{1}{M_\phi^2} \right) [m_{\eta'}^2(\tilde{c}_2 + \tilde{c}_1 - \tilde{c}_5) + 8\tilde{c}_3(2m_K^2 - m_\pi^2)] \left(\frac{\sqrt{2}\sin\theta_0}{F_8} - \frac{\cos\theta_8}{F_0} \right) \\
&+ \frac{4F_V^2}{\sqrt{3}} \left(\frac{1}{M_\rho^4} + \frac{1}{9M_\omega^4} \right) [\tilde{d}_1 m_{\eta'}^2 - \tilde{d}_3 m_{\eta'}^2 + 8\tilde{d}_2 m_\pi^2] \left(\frac{\sin\theta_0}{F_8} + \frac{\sqrt{2}\cos\theta_8}{F_0} \right) \\
&- \frac{8\sqrt{2}F_V^2}{9\sqrt{3}} \left(\frac{1}{M_\phi^4} \right) [\tilde{d}_1 m_{\eta'}^2 - \tilde{d}_3 m_{\eta'}^2 + 8\tilde{d}_2(2m_K^2 - m_\pi^2)] \left(\frac{\sqrt{2}\sin\theta_0}{F_8} - \frac{\cos\theta_8}{F_0} \right) \\
&+ \left(\frac{\cos\theta_8}{F_0} \right) \left[-8\sqrt{2}M_V F_V \tilde{c}_8 \left(\frac{1}{M_\rho^2} + \frac{1}{9M_\omega^2} + \frac{2}{9M_\phi^2} \right) \right. \\
&\quad \left. + 8F_V^2 M_V^2 \tilde{d}_5 \left(\frac{1}{M_\rho^4} + \frac{1}{9M_\omega^4} + \frac{2}{9M_\phi^4} \right) \right] \Big\}^2. \tag{65}
\end{aligned}$$

B The form factors of $\phi \rightarrow \eta\gamma^*$, $\eta \rightarrow \gamma\gamma^*$ and $\eta' \rightarrow \gamma\gamma^*$

The definition of the form factor is given in Eq.(15) and the explicit forms for different processes are reported below

$$\begin{aligned}
F_{\phi \rightarrow \eta\gamma^*}(s) &= \frac{1}{\cos(\theta_0 - \theta_8)} \left\{ \right. \\
&\frac{4\sqrt{2}}{3\sqrt{3}M_V M_\phi} \left(\frac{\sqrt{2}\cos\theta_0}{F_8} + \frac{\sin\theta_8}{F_0} \right) \times \\
&\times [M_\phi^2(\tilde{c}_2 - \tilde{c}_1 + \tilde{c}_5 - 2\tilde{c}_6) + m_\eta^2(\tilde{c}_2 + \tilde{c}_1 - \tilde{c}_5) + 8\tilde{c}_3(2m_K^2 - m_\pi^2) + (\tilde{c}_1 - \tilde{c}_2 + \tilde{c}_5)s] \\
&- \frac{8F_V}{3\sqrt{3}M_\phi} D_\phi(s) \left(\frac{\sqrt{2}\cos\theta_0}{F_8} + \frac{\sin\theta_8}{F_0} \right) [\tilde{d}_3(M_\phi^2 - m_\eta^2 + s) + \tilde{d}_1 m_\eta^2 + 8\tilde{d}_2(2m_K^2 - m_\pi^2)] \\
&\left. + \left(-\frac{\sin\theta_8}{F_0} \right) \left[-\frac{8M_V}{3M_\phi} \tilde{c}_8 + \frac{8\sqrt{2}F_V M_V^2}{3M_\phi} \tilde{d}_5 D_\phi(s) \right] \right\}, \tag{66}
\end{aligned}$$

where the definition of $D_R(s)$ is

$$D_R(s) = \frac{1}{M_R^2 - s - iM_R\Gamma_R(s)}. \tag{67}$$

For the narrow-width resonances ω, ϕ , we use the constant widths for them in the numerical discussion. For ρ resonance, the energy dependent width is constructed in the way introduced in [63]:

$$\Gamma_\rho(s) = \frac{sM_V}{96\pi F^2} [\sigma_\pi^3 \theta(s - 4m_\pi^2) + \frac{1}{2}\sigma_K^3 \theta(s - 4m_K^2)], \tag{68}$$

where $\sigma_P = \sqrt{1 - 4m_P^2/s}$ and $\theta(s)$ is the step function.

The form factors for $\eta \rightarrow \gamma\gamma^*$ and $\eta' \rightarrow \gamma\gamma^*$ are

$$\begin{aligned}
F_{\eta \rightarrow \gamma\gamma^*}(s) &= \frac{1}{\cos(\theta_0 - \theta_8)} \left\{ \right. \\
&- \frac{N_C}{12\sqrt{3}\pi^2} \left(\frac{\cos\theta_0}{F_8} - \frac{2\sqrt{2}\sin\theta_8}{F_0} \right) \\
&- \frac{2\sqrt{2}F_V}{\sqrt{3}M_V} \left(\frac{1}{M_\rho^2} + \frac{1}{9M_\omega^2} \right) \times \\
&\quad \left[m_\eta^2(\tilde{c}_2 + \tilde{c}_1 - \tilde{c}_5) + 8\tilde{c}_3 m_\pi^2 + (\tilde{c}_1 - \tilde{c}_2 + \tilde{c}_5)s \right] \left(\frac{\cos\theta_0}{F_8} - \frac{\sqrt{2}\sin\theta_8}{F_0} \right) \\
&- \frac{2\sqrt{2}F_V}{\sqrt{3}M_V} \left[D_\rho(s) + \frac{1}{9}D_\omega(s) \right] \times \\
&\quad \left[m_\eta^2(\tilde{c}_2 + \tilde{c}_1 - \tilde{c}_5) + 8\tilde{c}_3 m_\pi^2 + (\tilde{c}_2 + \tilde{c}_5 - \tilde{c}_1 - 2\tilde{c}_6)s \right] \left(\frac{\cos\theta_0}{F_8} - \frac{\sqrt{2}\sin\theta_8}{F_0} \right) \\
&+ \frac{8F_V}{9\sqrt{3}M_V} \left(\frac{1}{M_\phi^2} \right) \times \\
&\quad \left[m_\eta^2(\tilde{c}_2 + \tilde{c}_1 - \tilde{c}_5) + 8\tilde{c}_3(2m_K^2 - m_\pi^2) + (\tilde{c}_1 - \tilde{c}_2 + \tilde{c}_5)s \right] \left(\frac{\sqrt{2}\cos\theta_0}{F_8} + \frac{\sin\theta_8}{F_0} \right) \\
&+ \frac{8F_V}{9\sqrt{3}M_V} D_\phi(s) \left(\frac{\sqrt{2}\cos\theta_0}{F_8} + \frac{\sin\theta_8}{F_0} \right) \times \\
&\quad \left[m_\eta^2(\tilde{c}_2 + \tilde{c}_1 - \tilde{c}_5) + 8\tilde{c}_3(2m_K^2 - m_\pi^2) + (\tilde{c}_2 + \tilde{c}_5 - \tilde{c}_1 - 2\tilde{c}_6)s \right] \\
&+ \frac{4F_V^2}{\sqrt{3}} \left[\frac{1}{M_\rho^2} D_\rho(s) + \frac{1}{9M_\omega^2} D_\omega(s) \right] \left[\tilde{d}_1 m_\eta^2 + \tilde{d}_3(s - m_\eta^2) + 8\tilde{d}_2 m_\pi^2 \right] \left(\frac{\cos\theta_0}{F_8} - \frac{\sqrt{2}\sin\theta_8}{F_0} \right) \\
&- \frac{8\sqrt{2}F_V^2}{9\sqrt{3}} \left[\frac{1}{M_\phi^2} D_\phi(s) \right] \left[\tilde{d}_1 m_\eta^2 + \tilde{d}_3(s - m_\eta^2) + 8\tilde{d}_2(2m_K^2 - m_\pi^2) \right] \left(\frac{\sqrt{2}\cos\theta_0}{F_8} + \frac{\sin\theta_8}{F_0} \right) \\
&+ \left(-\frac{\sin\theta_8}{F_0} \right) \left[-4\sqrt{2}M_V F_V \tilde{c}_8 \left(D_\rho(s) + \frac{1}{M_\rho^2} + \frac{1}{9}D_\omega(s) + \frac{1}{9M_\omega^2} + \frac{2}{9}D_\phi(s) + \frac{2}{9M_\phi^2} \right) \right. \\
&\quad \left. + 8F_V^2 M_V^2 \tilde{d}_5 \left(\frac{1}{M_\rho^2} D_\rho(s) + \frac{1}{9M_\omega^2} D_\omega(s) + D_\phi(s) \frac{2}{9M_\phi^2} \right) \right] \left. \right\}, \tag{69}
\end{aligned}$$

$$\begin{aligned}
F_{\eta' \rightarrow \gamma \gamma^*}(s) &= \frac{1}{\cos(\theta_0 - \theta_8)} \left\{ \right. \\
&- \frac{N_C}{12\sqrt{3}\pi^2} \left(\frac{\sin \theta_0}{F_8} + \frac{2\sqrt{2} \cos \theta_8}{F_0} \right) \\
&- \frac{2\sqrt{2} F_V}{\sqrt{3} M_V} \left(\frac{1}{M_\rho^2} + \frac{1}{9M_\omega^2} \right) \times \\
&\quad \left[m_{\eta'}^2 (\tilde{c}_2 + \tilde{c}_1 - \tilde{c}_5) + 8\tilde{c}_3 m_\pi^2 + (\tilde{c}_1 - \tilde{c}_2 + \tilde{c}_5) s \right] \left(\frac{\sin \theta_0}{F_8} + \frac{\sqrt{2} \cos \theta_8}{F_0} \right) \\
&- \frac{2\sqrt{2} F_V}{\sqrt{3} M_V} \left[D_\rho(s) + \frac{1}{9} D_\omega(s) \right] \times \\
&\quad \left[m_{\eta'}^2 (\tilde{c}_2 + \tilde{c}_1 - \tilde{c}_5) + 8\tilde{c}_3 m_\pi^2 + (\tilde{c}_2 + \tilde{c}_5 - \tilde{c}_1 - 2\tilde{c}_6) s \right] \left(\frac{\sin \theta_0}{F_8} + \frac{\sqrt{2} \cos \theta_8}{F_0} \right) \\
&+ \frac{8 F_V}{9\sqrt{3} M_V} \left(\frac{1}{M_\phi^2} \right) \left(\frac{\sqrt{2} \sin \theta_0}{F_8} - \frac{\cos \theta_8}{F_0} \right) \times \\
&\quad \left[m_{\eta'}^2 (\tilde{c}_2 + \tilde{c}_1 - \tilde{c}_5) + 8\tilde{c}_3 (2m_K^2 - m_\pi^2) + (\tilde{c}_1 - \tilde{c}_2 + \tilde{c}_5) s \right] \\
&+ \frac{8 F_V}{9\sqrt{3} M_V} D_\phi(s) \left(\frac{\sqrt{2} \sin \theta_0}{F_8} - \frac{\cos \theta_8}{F_0} \right) \times \\
&\quad \left[m_{\eta'}^2 (\tilde{c}_2 + \tilde{c}_1 - \tilde{c}_5) + 8\tilde{c}_3 (2m_K^2 - m_\pi^2) + (\tilde{c}_2 + \tilde{c}_5 - \tilde{c}_1 - 2\tilde{c}_6) s \right] \\
&+ \frac{4F_V^2}{\sqrt{3}} \left[\frac{1}{M_\rho^2} D_\rho(s) + \frac{1}{9M_\omega^2} D_\omega(s) \right] \left[\tilde{d}_1 m_{\eta'}^2 + \tilde{d}_3 (s - m_{\eta'}^2) + 8\tilde{d}_2 m_\pi^2 \right] \left(\frac{\sin \theta_0}{F_8} + \frac{\sqrt{2} \cos \theta_8}{F_0} \right) \\
&- \frac{8\sqrt{2} F_V^2}{9\sqrt{3}} \left[\frac{1}{M_\phi^2} D_\phi(s) \right] \left[\tilde{d}_1 m_{\eta'}^2 + \tilde{d}_3 (s - m_{\eta'}^2) + 8\tilde{d}_2 (2m_K^2 - m_\pi^2) \right] \left(\frac{\sqrt{2} \sin \theta_0}{F_8} - \frac{\cos \theta_8}{F_0} \right) \\
&+ \left(\frac{\cos \theta_8}{F_0} \right) \left[-4\sqrt{2} M_V F_V \tilde{c}_8 \left(D_\rho(s) + \frac{1}{M_\rho^2} + \frac{1}{9} D_\omega(s) + \frac{1}{9M_\omega^2} + \frac{2}{9} D_\phi(s) + \frac{2}{9M_\phi^2} \right) \right. \\
&\quad \left. + 8F_V^2 M_V^2 \tilde{d}_5 \left(\frac{1}{M_\rho^2} D_\rho(s) + \frac{1}{9M_\omega^2} D_\omega(s) + D_\phi(s) \frac{2}{9M_\phi^2} \right) \right] \left. \right\}. \tag{70}
\end{aligned}$$

C The decay widths of $V \rightarrow Pl^-l^+$, $P \rightarrow Vl^-l^+$ and $P \rightarrow \gamma l^-l^+$

The kinematic variables used in this sector are defined below.

- For $V(p) \rightarrow l^-(k_1) l^+(k_2) P(q)$

$$\begin{aligned}
k &= k_1 + k_2, \\
(k_1 + k_2)^2 &= s, \\
(q + k_2)^2 &= t.
\end{aligned} \tag{71}$$

The general decay amplitude is

$$T(V \rightarrow l^- l^+ P) = e^2 \epsilon_{\mu\nu\rho\sigma} \epsilon_p^\nu k^\rho p^\sigma \bar{u}(k_1) \gamma^\mu v(k_2) A_{V \rightarrow l^- l^+ P}(s, t). \tag{72}$$

To calculate the decay width, one needs

$$\begin{aligned}
& |\epsilon_{\mu\nu\rho\sigma}\epsilon_p^\nu k^\rho p^\sigma \bar{u}(k_1)\gamma^\mu v(k_2)|^2 = \\
& 2m_l^4 s + 2m_l^2 [m_P^4 + M_V^4 - M_V^2 s - m_P^2(2M_V^2 + s) - 2s t] \\
& + s [m_P^4 + M_V^4 + s^2 + 2s t + 2t^2 - 2m_P^2(s + t) - 2M_V^2(s + t)].
\end{aligned} \tag{73}$$

Then the decay width is found to be

$$\Gamma_{V \rightarrow Pl^- l^+} = \frac{1}{3} \frac{1}{8\pi^3} \frac{1}{32 M_V} \int_{4m_l^2}^{(M_V - m_P)^2} ds \int_{t_{\min}}^{t_{\max}} dt |T(s, t)|^2 \tag{74}$$

where

$$\begin{aligned}
t_{\min} &= \frac{M_V^2 + m_P^2 + 2m_l^2 - s}{2} - \frac{\sqrt{s(s - 4m_l^2)[s - (M_V + m_P)^2][s - (M_V - m_P)^2]}}{2s}, \\
t_{\max} &= \frac{M_V^2 + m_P^2 + 2m_l^2 - s}{2} + \frac{\sqrt{s(s - 4m_l^2)[s - (M_V + m_P)^2][s - (M_V - m_P)^2]}}{2s}.
\end{aligned} \tag{75}$$

- For $P(q) \rightarrow l^-(k_1) l^+(k_2) V(p)$

$$\begin{aligned}
k &= k_1 + k_2, \\
(k_1 + k_2)^2 &= s, \\
(p + k_2)^2 &= t,
\end{aligned} \tag{76}$$

The general decay amplitude is

$$T(P \rightarrow l^- l^+ V) = e^2 \epsilon_{\mu\nu\rho\sigma} \epsilon_p^\nu k^\rho p^\sigma \bar{u}(k_1) \gamma^\mu v(k_2) A_{P \rightarrow l^- l^+ V}(s, t). \tag{77}$$

To calculate the decay width, one needs

$$\begin{aligned}
& |\epsilon_{\mu\nu\rho\sigma}\epsilon_p^\nu k^\rho p^\sigma \bar{u}(k_1)\gamma^\mu v(k_2)|^2 = \\
& 2m_l^4 s + 2m_l^2 [m_P^4 + M_V^4 - M_V^2 s - m_P^2(2M_V^2 + s) - 2s t] \\
& + s [m_P^4 + M_V^4 + s^2 + 2s t + 2t^2 - 2m_P^2(s + t) - 2M_V^2(s + t)].
\end{aligned} \tag{78}$$

The decay width is

$$\Gamma_{P \rightarrow Vl^- l^+} = \frac{1}{8\pi^3} \frac{1}{32 m_P} \int_{4m_l^2}^{(m_P - M_V)^2} ds \int_{t_{\min}}^{t_{\max}} dt |T(s, t)|^2 \tag{79}$$

where

$$\begin{aligned}
t_{\min} &= \frac{M_V^2 + m_P^2 + 2m_l^2 - s}{2} - \frac{\sqrt{s(s - 4m_l^2)[s - (M_V + m_P)^2][s - (M_V - m_P)^2]}}{2s}, \\
t_{\max} &= \frac{M_V^2 + m_P^2 + 2m_l^2 - s}{2} + \frac{\sqrt{s(s - 4m_l^2)[s - (M_V + m_P)^2][s - (M_V - m_P)^2]}}{2s}.
\end{aligned} \tag{80}$$

- For $P(p) \rightarrow l^-(k_{21}) l^+(k_{22}) \gamma(k_1)$

$$\begin{aligned}
k_2 &= k_{21} + k_{22}, \\
(k_{21} + k_{22})^2 &= s, \\
(k_1 + k_{22})^2 &= t.
\end{aligned} \tag{81}$$

The general decay amplitude is

$$T(P \rightarrow l^- l^+ \gamma) = e^3 \epsilon_{\mu\nu\rho\sigma} \epsilon_1^\nu k_1^\rho k_2^\sigma \bar{u}(k_{21}) \gamma^\mu v(k_{22}) A_{P \rightarrow l^- l^+ \gamma}(s, t). \tag{82}$$

To calculate the decay width, one needs

$$\begin{aligned}
&|\epsilon_{\mu\nu\rho\sigma} \epsilon_1^\nu k_1^\rho k_2^\sigma \bar{u}(k_{21}) \gamma^\mu v(k_{22})|^2 = \\
&2m_l^4 s + 2m_l^2 (m_P^4 - m_P^2 s - 2st) + s[m_P^4 + s^2 + 2st + 2t^2 - 2m_P^2(s+t)].
\end{aligned} \tag{83}$$

The decay width is

$$\Gamma_{P \rightarrow \gamma l^- l^+} = \frac{1}{8\pi^3} \frac{1}{32 m_P} \int_{4m_l^2}^{m_P^2} ds \int_{t_{\min}}^{t_{\max}} dt |T(s, t)|^2 \tag{84}$$

where

$$\begin{aligned}
t_{\min} &= \frac{m_P^2 + 2m_l^2 - s}{2} - \frac{(m_P^2 - s)\sqrt{s(s - 4m_l^2)}}{2s}, \\
t_{\max} &= \frac{m_P^2 + 2m_l^2 - s}{2} + \frac{(m_P^2 - s)\sqrt{s(s - 4m_l^2)}}{2s}.
\end{aligned} \tag{85}$$

The explicit expressions of the decay amplitudes are given below

$$\begin{aligned}
T(\omega \rightarrow \pi l^- l^+) &= -e^2 \epsilon_{\mu\nu\rho\sigma} \epsilon_p^\nu k^\rho p^\sigma \bar{u}(k_1) \gamma^\mu v(k_2) \frac{1}{s} \left\{ \right. \\
&\quad - \frac{2\sqrt{2}}{F_\pi M_V M_\omega} [(\tilde{c}_1 + \tilde{c}_2 + 8\tilde{c}_3 - \tilde{c}_5)m_\pi^2 + (\tilde{c}_2 + \tilde{c}_5 - \tilde{c}_1 - 2\tilde{c}_6)M_\omega^2 + (\tilde{c}_1 - \tilde{c}_2 + \tilde{c}_5)s] \\
&\quad \left. + \frac{4F_V}{F_\pi M_\omega} D_\rho(s) [(\tilde{d}_1 + 8\tilde{d}_2 - \tilde{d}_3)m_\pi^2 + \tilde{d}_3(M_\omega^2 + s)] \right\},
\end{aligned} \tag{86}$$

$$\begin{aligned}
T(\rho \rightarrow \pi l^- l^+) &= -e^2 \epsilon_{\mu\nu\rho\sigma} \epsilon_p^\nu k^\rho p^\sigma \bar{u}(k_1) \gamma^\mu v(k_2) \frac{1}{s} \left\{ \right. \\
&\quad - \frac{2\sqrt{2}}{3F_\pi M_V M_\rho} [(\tilde{c}_1 + \tilde{c}_2 + 8\tilde{c}_3 - \tilde{c}_5)m_\pi^2 + (\tilde{c}_2 + \tilde{c}_5 - \tilde{c}_1 - 2\tilde{c}_6)M_\rho^2 + (\tilde{c}_1 - \tilde{c}_2 + \tilde{c}_5)s] \\
&\quad \left. + \frac{4F_V}{3F_\pi M_\rho} D_\omega(s) [(\tilde{d}_1 + 8\tilde{d}_2 - \tilde{d}_3)m_\pi^2 + \tilde{d}_3(M_\rho^2 + s)] \right\},
\end{aligned} \tag{87}$$

$$T(\phi \rightarrow \eta l^- l^+) = -e^2 \epsilon_{\mu\nu\rho\sigma} \epsilon_1^\nu k_1^\rho k_2^\sigma \bar{u}(k_1) \gamma^\mu v(k_2) \frac{1}{s} F_{\phi \rightarrow \eta \gamma^*}(s), \quad (88)$$

$$\begin{aligned} T(\pi \rightarrow \gamma l^- l^+) &= e^3 \epsilon_{\mu\nu\rho\sigma} \epsilon_1^\nu k_1^\rho k_2^\sigma \bar{u}(k_{21}) \gamma^\mu v(k_{22}) \frac{1}{s} \left\{ \right. \\ &\quad - \frac{N_C}{12\pi^2 F_\pi} - \frac{2\sqrt{2}F_V}{3F_\pi M_V} \left(\frac{1}{M_\rho^2} + \frac{1}{M_\omega^2} \right) [(\tilde{c}_1 + \tilde{c}_2 + 8\tilde{c}_3 - \tilde{c}_5)m_\pi^2 + (\tilde{c}_1 - \tilde{c}_2 + \tilde{c}_5)s] \\ &\quad - \frac{2\sqrt{2}F_V}{3F_\pi M_V} [D_\rho(s) + D_\omega(s)] [(\tilde{c}_1 + \tilde{c}_2 + 8\tilde{c}_3 - \tilde{c}_5)m_\pi^2 + (\tilde{c}_2 + \tilde{c}_5 - \tilde{c}_1 - 2\tilde{c}_6)s] \\ &\quad \left. + \frac{4F_V^2}{3F_\pi} \left[\frac{1}{M_\rho^2} D_\omega(s) + \frac{1}{M_\omega^2} D_\rho(s) \right] [(\tilde{d}_1 + 8\tilde{d}_2 - \tilde{d}_3)m_\pi^2 + \tilde{d}_3 s] \right\} \quad (89) \end{aligned}$$

$$T(\eta \rightarrow \gamma l^- l^+) = e^3 \epsilon_{\mu\nu\rho\sigma} \epsilon_1^\nu k_1^\rho k_2^\sigma \bar{u}(k_{21}) \gamma^\mu v(k_{22}) \frac{1}{s} F_{\eta \rightarrow \gamma \gamma^*}(s), \quad (90)$$

$$T(\eta' \rightarrow \gamma l^- l^+) = e^3 \epsilon_{\mu\nu\rho\sigma} \epsilon_1^\nu k_1^\rho k_2^\sigma \bar{u}(k_{21}) \gamma^\mu v(k_{22}) \frac{1}{s} F_{\eta' \rightarrow \gamma \gamma^*}(s). \quad (91)$$

where $F_{\eta \rightarrow \gamma \gamma^*}$ and $F_{\eta' \rightarrow \gamma \gamma^*}$ are given in Eqs.(69) and (70).

References

- [1] G. Amelino-Camelia, *et al.*, Eur. Phys. J. **C68** (2010) 619.
- [2] L. P. Gan, and A. Gasparian, PoS **CD09** (2009) 048. And also the contribution from M. Kunkel that is about to appear in the proceeding of HADRON 2011.
- [3] H. B. Li, J. Phys. **G36** (2009) 085009.
- [4] J. Gasser and H. Leutwyler, Annals Phys. **158**, 142 (1984); J. Gasser and H. Leutwyler, Nucl. Phys. B **250** (1985) 465.
- [5] A. Pich, Rept. Prog. Phys. **58** (1995) 563; G. Ecker, Prog. Part. Nucl. Phys. **35** (1995)1.
- [6] G. t'Hooft, Nucl. Phys. **B72** (1974) 461; E. Witten, Nucl. Phys. **B156** (1979) 269; S. Coleman and E. Witten, Phys. Rev. Lett. **45** (1980) 100; G. Veneziano, Phys. Lett. **B95** (1980) 90.
- [7] R. Kaiser and H. Leutwyler, Eur. Phys. J. **C 17** (2000) 623.
- [8] P. Herrera-Siklody, J. I. Latorre, P. Pascual and J. Taron, Nucl. Phys. **B 497** (1997) 345.
- [9] P. Herrera-Siklody, J. I. Latorre, P. Pascual and J. Taron, Phys. Lett. **B 419** (1998) 326.
- [10] H. Leutwyler, Nucl. Phys. Proc. Suppl. **64** (1998) 223.
- [11] R. Kaiser and H. Leutwyler, arXiv: hep-ph/9806336.
- [12] K. Nakamura, *et al.*, J. Phys. G **37**, 075021 (2010).

- [13] R. Escribano, P. Masjuan and J. J. Sanz-Cillero, JHEP **1105** (2011) 094.
- [14] G. Ecker, J. Gasser, A. Pich and E. de Rafael, Nucl. Phys. **B321** (1989) 311.
- [15] S. Peris, M. Perrottet and E. de Rafael, JHEP **9805** (1998) 011; M. Knecht, S. Peris, M. Perrottet and E. de Rafael, Phys. Rev. Lett. **83** (1999) 5230; S. Peris, B. Phily and E. de Rafael, Phys. Rev. Lett. **86** (2001) 14.
- [16] K. Kampf and B. Moussallam, Eur. Phys. J. **C47** (2006) 723.
- [17] Z. H. Guo and J. J. Sanz-Cillero, Phys. Rev. **D79** (2009) 096006;
- [18] Z. H. Guo, Phys. Rev. **D78** (2008) 033004.
- [19] D. Gomez Dumm, P. Roig, A. Pich and J. Portoles, Phys. Rev. **D81** (2010) 034031.
- [20] Z. H. Guo and P. Roig, Phys. Rev. **D82** (2010) 113016.
- [21] B. Moussallam, Phys. Rev. **D51** (1995) 4939.
- [22] B. Moussallam, Nucl. Phys. **B504** (1997) 381.
- [23] J. Bijnens, E. Gamiz, E. Lipartia and J. Prades, JHEP **0304** (2003) 055.
- [24] M. Knecht and A. Nyffeler, Eur. Phys. J. **C21** (2001) 659.
- [25] P. D. Ruiz-Femenia, A. Pich and J. Portoles, JHEP **0307** (2003) 003
- [26] For the review see: T. Feldmann, Int. J. Mod. Phys. **A15** (2000) 159.
- [27] C. Degrande and J.-M. Gerard, JHEP **0905** (2009) 043.
- [28] V. Mathieu and V. Vento, Phys. Lett. **B688** (2010) 314.
- [29] T. Feldmann and P. Kroll, Phys. Lett. **B 413**, 410 (1997).
- [30] T. Feldmann, P. Kroll and B. Stech, Phys. Rev. **D 58** (1998) 114006.
- [31] T. Feldmann, P. Kroll and B. Stech, Phys. Lett. **B 449** (1999) 339.
- [32] P. Ball, J. M. Frere and M. Tytgat, Phys. Lett. **B 365**, 367 (1996).
- [33] R. Escribano and J.M. Frere, Phys. Lett. **B 459**, 288 (1999).
- [34] F.De Fazio and M.R. Pennington, JHEP **07**, 051 (2000).
- [35] M. Benayoun, L. DelBuono and H. B. O'Connell, Eur. Phys. J. **C 17** (2000) 593.
- [36] J. L. Goity, A. M. Bernstein and B. R. Holstein, Phys. Rev. **D66** (2002) 076014.
- [37] A.Bramon, R. Escribano, and M.D. Scadron, Phys. Lett. **B 503**, 271 (2001).
- [38] R. Escribano and J. M. Frere, JHEP **0506** (2005) 029.
- [39] T. N. Pham, Phys. Lett. **B694** (2010) 129.

- [40] R. Kaiser, arXiv: hep-ph/0502065.
- [41] V. Cirigliano, G. Ecker, M. Eidemuller, R. Kaiser, A. Pich and J. Portoles, Nucl. Phys. **B753** (2006) 139.
- [42] J. Wess and B. Zumino, Phys. Lett. **B37** (1971) 95.
- [43] E. Witten, Nucl. Phys. **B223** (1983) 422.
- [44] G. Ecker, J. Gasser, H. Leutwyler, A. Pich and E. de Rafael, Phys. Lett. B **223** (1989) 425.
- [45] K. Kampf and J. Novotny, Phys. Rev. D **84** (2011) 014036.
- [46] G. P. Lepage and S. J. Brodsky, Phys. Lett. B **87** (1979) 359; S. J. Brodsky and G. P. Lepage, Phys. Rev. D **24** (1981) 1808.
- [47] A. V. Manohar, Phys. Lett. **B244** (1990) 101.
- [48] J. M. Gerard and T. Lahna, Phys. Lett. **B356** (1995) 381.
- [49] V. Mateu and J. Portoles, Eur. Phys. J. C **52**, 325 (2007).
- [50] A. Pich, I. Rosell and J. J. Sanz-Cillero, JHEP **1102** (2011) 109.
- [51] Z. H. Guo, J. J. Sanz-Cillero and H. Q. Zheng, JHEP **0706** (2007) 030.
- [52] Z. H. Guo and J. A. Oller, Phys. Rev. D **84** (2011) 034005.
- [53] A. Etkin, *et al.*, Phys. Rev. D **25** (1982) 1786.
- [54] Lepton-G Coll. R. I. Dzhelyadin *et al.*, Phys. Lett. B **94**, 548 (1980).
- [55] Lepton-G Coll. R. I. Dzhelyadin *et al.*, Phys. Lett. B **88**, 379 (1979).
- [56] CELLO Coll. H.-J. Behrend *et al.*, Z. Phys. **C49** (1991) 401.
- [57] M.N. Achasov *et al.*, Phys. Lett. B **504**, 275 (2001).
- [58] R. Arnaldi *et al.*, Phys. Lett. B **677**, 260 (2009).
- [59] TPC/ 2γ Coll. H. Aihara *et al.*, Phys. Rev. Lett. **64** (1990) 172.
- [60] M. Acciarri *et al.*, Phys. Lett. B **418**, 399 (1998).
- [61] P. Roig, Nucl. Phys. Proc. Suppl. **207-208** (2010) 145.
- [62] J. Bijnens, L. Girlanda and P. Talavera, Eur. Phys. J. C **23** (2002) 539.
- [63] D. Gomez Dumm, A. Pich and J. Portoles, Phys. Rev. D **62** (2000) 054014.